IEEE Access
Multidisciplinary | Rapid Review | Open Access Journal

Received May 9, 2020, accepted May 22, 2020, date of publication June 9, 2020, date of current version June 22, 2020.

Digital Object Identifier 10.1109/ACCESS.2020.3001052

Spatial Modeling of Interference in Inter-Vehicular Communications for 3-D Volumetric Wireless Networks

ALI RAZA[1], SYED JUNAID NAWAZ[1], (Senior Member, IEEE), SHURJEEL WYNE[1], (Senior Member, IEEE), ABRAR AHMED[1], MUHAMMAD AWAIS JAVED[1], (Senior Member, IEEE), AND MOHAMMAD N. PATWARY[2], (Senior Member, IEEE)

[1]Department of Electrical and Computer Engineering, COMSATS University Islamabad (CUI), Islamabad 45550, Pakistan
[2]School of Computing and Digital Technology, Birmingham City University, Birmingham B5 5JU, U.K.

Corresponding author: Syed Junaid Nawaz (junaidnawaz@ieee.org)

This work was supported by the Higher Education Commission (HEC), Pakistan, under Project 21-1934-SRGP-R&D-HEC-18 and Project 21-2180-SRGP-R&D-HEC-19.

ABSTRACT Unmanned aerial vehicle (UAV) assisted cell-free communications hold promise for enhancing the coverage and capacity of heterogeneous cellular networks. However, the network interference in such scenarios must be accurately modeled for efficient system design. The spatial characteristics of the desired and interfering signals can be jointly modeled by considering the characteristics of the signal-to-interference ratio (SIR). This work proposes a generalized framework for modeling the spatial statistics of the SIR encountered in 3-D volumetric inter-vehicular communication channels. Though the novel paradigm of UAV-assisted cell-free vehicular communications is analyzed in particular, the proposed framework is more general in that it incorporates 3-D mobility at both link ends. Also, this framework is shown to include as its special cases, several notable 2-D propagation models of network interference including those for terrestrial vehicle-to-vehicle and fixed-to-vehicle scenarios. Analytical expressions are derived for the SIR level-crossing-rate (LCR), average-fade-duration (AFD), spatial auto-covariance (SAC), and coherence distance (CD). Both single- and multi-cluster scattering environments are analyzed and the impact of channel parameters such as the direction and velocity of mobile nodes as well as the altitudes of the UAV and scattering cluster(s) on the SIR fading statistics is investigated. Finally, some future extensions of this work are also discussed such as the integration of intelligent reflective surfaces in the propagation scenario to generate favorable channel conditions.

INDEX TERMS Channel modeling, cell-free communications, fading, interference, inter-vehicular, signal-to-interference ratio, second-order statistics, unmanned aerial vehicle (UAV).

I. INTRODUCTION

The deployment of the 5th generation (5G) of cellular networks commenced with Release-15 of the 3rd generation partnership project (3GPP) [1] and it is set to gain momentum with the 3GPP Release-16 expected during the year 2020 [2], [3]. The 5G incorporates several revolutionary technologies such as massive multiple-input multiple-output (mMIMO), small cells, millimeter wave (mmWave), mobile edge computing (MEC), and software-defined networking (SDN) – to name a few. These innovations are expected to facilitate massive machine type communications (mMTC), enhanced mobile broadband (eMBB), and ultra-reliable low-latency communications (URLLC) [4].

The 5G networks have necessitated a three dimensional (3-D) volumetric modeling of the propagation channel due to the provision of unmanned aerial vehicles (UAVs) serving as base stations (BSs) [5] as well as small-cells that have rich scattering at both link-ends. Thus 5G has extended the conventional concept of two dimensional (2-D) terrestrial networks to 3-D volumetric networks.

The associate editor coordinating the review of this manuscript and approving it for publication was Jiayi Zhang.

A. SIGNIFICANCE OF 3-D SPATIAL STATISTICS IN 5G COMMUNICATIONS

The combination of small-cells and mMTC in 5G networks is expected to incur increased inter-tier interference due to an aggressive frequency reuse in these ultra-dense 5G heterogeneous networks (HetNets). However, this network interference can be mitigated by deploying large-scale multi-antenna systems that provide a very fine 3-D angular resolution of the multipath [6]–[8]. For example, the channel capacity can be increased by exploiting knowledge of the angular statistics of the desired and interference signals for beam-steering and null-steering, respectively. The useful and interference channels can be jointly characterized by investigating the statistics of the signal-to-interference ratio (SIR) [6]. Thus, 3-D angular modeling of the interference is necessary for an accurate performance characterization of the volumetric vehicle-to-vehicle (V2V) 5G networks. Such V2V communication scenarios include aerial-vehicle-to-aerial-vehicle (AV2AV), aerial-vehicle-to-ground-vehicle (AV2GV), and ground-Vehicle-to-ground-vehicle (GV2GV) communications. Airborne internet access through mesh network topology between the aerial vehicular nodes is a notable emerging example of AV2AV communications [9].

The spatial statistics of the radio channels are useful in deriving second order fading statistics such as the level-crossing-rate (LCR), average-fade-duration (AFD), spatial auto-covariance (SAC) and the coherence distance (CD) [10]. LCR is defined as the measure of the average rate at which the given signal envelope crosses a threshold level, where the AFD is defined as the average duration for which the signal envelope stays below the threshold level. SAC represents the correlation of the received signals at different spatial positions along the mobility route of communicating nodes, while CD determines the maximum spatial separation between two points over which the normalized correlation coefficient remain higher than a minimum defined level (e.g., $\geq$ 50%). In [11], a 2-D V2V channel was considered and analytical expressions for the second-order fading statistics were derived that independently investigate the desired channel or the interference channel only. In [12]–[15] and [16], the authors derived analytical expressions for second-order fading statistics by using spatio-temporal correlation functions for Nakagami-q and Rician fading channels, respectively, which can be used to independently study desired or interference channels.

As the research interest in mMIMO has increased [17], [18], the 3-D angular characterization of the desired and interference signals has become an essential task [19]. In previous cellular network generations, the cell-users were typically located far from the BS such that the elevation angle could be neglected and an azimuth-only channel characterization sufficed for predicting network performance. However, due to the presence of small cells with reduced coverage area and UAV BSs in 5G networks, the elevation angle needs to be considered, which necessitates a full 3-D spatial characterization of the desired and interference channels.

B. MULTI-ANTENNA INTEGRATED CELL-FREE INTER-VEHICULAR COMMUNICATIONS

Recently, cell-free communications have been proposed to meet the capacity demands of emerging wireless networks [2], [20]. Such cell-free communications may build either on UAV BSs or on distributed multi-antenna systems. In [21], the authors thoroughly reviewed the potential benefits and challenges of UAV-based cell-free (also referred as fluid cells) communications, whereas cell-free communications based on small cells was discussed in [22]. In [23], a UAV-assisted cell-free mMIMO communications architecture was proposed, whereas the authors in [24] proposed mMIMO communications for providing long-range connectivity and space division multiple access to the highly mobile UAV network nodes. To quantify the benefits of cell-free mMIMO systems in terms of energy- and cost-efficiency, the authors in [25] provided a comprehensive survey of cell-free mMIMO systems. Some signal processing based manipulations for decreasing the fronthaul responsibilities in terms of joint channel estimation and precoding are proposed. The authors in [26] study the statistics of mixed radiofrequency/free-space optical (RF/FSO) relay systems for V2V networks. The channel is modeled as gamma-gamma (G-G) and product of Nakagami-m and G-G of mixed RF/FSO relay systems and study the second-order statistics of infrastructure-to-infrastructure (I2I) FSO links and the RF/FSO/RF V2V cascaded relay links. In particular, the closed-form analytical expressions for cumulative distribution function (CDF), LCR, and AFD using different propagation models are derived. In [27], [28], the authors analyzed the performance of the relay-assisted vehicular networks. The outage probability and bit error rate (BER) expressions are derived with a formulation of the power allocation problem and the authors optimized the power allocation values to minimize BER. Data-driven approaches (e.g., machine learning) has recently received a significant research interest for providing solutions to various challenges in wireless communication networks as an alternative to the mathematical models-based algorithmic solutions [2]. In [29], the authors proposed a practical solution for channel estimation in cell-free mmWave mMIMO systems by deploying a fast and flexible denoising convolutional neural network (FFDCNN) based solution.

In [30], stochastic geometry was used to analyze the interference in directional UAV communications. In summary, characterizing the network interference in angular domain as well as investigating the channel's second-order fading statistics are important for good transceiver design in vehicular cell-free communications.

C. MULTIPATH SHAPE FACTORS AND FADING STATISTICS OF INTERFERENCE

The higher-order statistics (HOS) of wireless channels are regarded as important for modeling and studying of wireless communication systems. In [31], characterization of HoS of channel capacity for κ-μ and κ-μ shadowed fading channel

are studied. In wireless communications, multipath shape factors are acquainted with the representation of first and second-order statistics of the received signal fluctuations. In [10], the authors proposed a theory of multipath shape factors for analyzing the small-scale fading for fixed-to-vehicle (F2V) radio propagation channels. The authors used these shape factors to derive analytical expressions for the second-order fading statistics of a Rayleigh fading channel assuming radio propagation in the 2-D azimuthal plane. This theory was revisited in [32] and [33] for Rician and Nakagami-*m* fading channels, respectively. In [34], the authors extended the multipath shape factor theory, previously proposed for 2-D propagation, to 3-D multipath propagation in a F2V communication setting. In [35], the authors further generalized the multipath shape factor theory by considering a 3-D geometry for vehicle-to-vehicle communications and jointly exploiting the 3-D angle-of-arrival (AoA) and angle-of-departure (AoD) of the multipath. It is noteworthy that the work in [35] includes all previous proposals on the multipath shape factors as its special cases.

In [10], the authors used the theory of 2-D multipath shape factors to model the network interference by an interference azimuth spectrum (IAS). The IAS was utilized to jointly characterize the fading statistics of the desired and the interference channels in terms of the SIR. This work was extended to 3-D space in [6] and analytical expressions were derived for the second-order fading statistics of SIR in terms of LCR, AFD, and CD. In [36], the authors jointly investigated the fading statistics of the interference and desired channels for a F2V communication scenario. Although the work in [36] claimed to model interference for vehicle-to-everything (V2X) communications, i.e., inclusive of mobility at both link ends, the actual expressions derived in that work were restricted to the F2V communication case only. To the best of the author's knowledge, spatial modeling and second-order fading statistics of the SIR in 3-D volumetric inter-vehicular communication channels have not been previously reported in the literature.

D. CONTRIBUTIONS AND ORGANIZATION

This work proposes an analytical framework for modeling the network interference in 3-D spatial domain for ultra-dense HetNets. In contrast to the work of [6], [36], the proposed framework can accommodate 3-D node-mobility at both ends of the communication link, i.e., node-mobility in both the horizontal and the vertical planes can be considered. Different to the work in [37], the proposed work jointly investigates the second-order fading statistics of interference and desired channels in terms of SIR. Also, in [37], Rayleigh distribution is considered to model the channel fading behaviour, while it is modeled as Nakagami-*m* distributed in the proposed work which is a more generalized consideration. The proposed generalized framework is flexible enough to model several interesting scenarios in emerging wireless networks, e.g., the communication channel between a UAV BS and a terrestrial vehicular node can be modeled, which was not possible with previously reported models. For the reader's benefit, Table 1 briefly summarizes the notable literature on angular modeling of interference in wireless networks, where the contributions of this work are also briefly highlighted. The main contributions of this work are listed as follows:

- An analytical framework for modeling the network interference in 3-D angular domain for inter-vehicular volumetric communication networks is proposed.
- Analytical expressions for jointly (in terms of SIR) characterizing the second-order fading statistics of desired (main) and interference channels are derived. The considered quantifiers for second-order fading statistics are LCR, AFD, SAC, and CD.
- The impact of various physical channel parameters on the channel second-order fading statistics with respect to SIR is thoroughly investigated. Moreover, emerging inter-vehicular communication scenarios are studied, e.g., UAV to ground vehicle communications.

The rest of this paper is organized as follows. Section II presents the considered system model. Section III presents the derivation of second-order fading statistics of 3-D volumetric inter-vehicular communication networks. In Section IV, the conducted simulations, obtained results, and related discussions are provided. Finally, the paper is concluded in Section V.

II. SYSTEM MODEL

The considered inter-vehicular 3-D volumetric HetNet is illustrated in Fig. 1. This figure shows the communication networks between different vehicular nodes, where AV2GV links are mainly focused. The aerial vehicular (AV) and ground vehicular (GV) nodes are labeled as AV_q and GV_p, respectively, where q and p represent the node indices. A fixed ground BS (GBS_f) provides the backhaul links to AV nodes, which is indicated as fixed-to-aerial vehicular (F2AV) links in the figure. The basic definition of the main physical parameters of the proposed model is given in Table 2. In such HetNets the aggressive reuse of radio resources and dense network connectivity causes an increased level of network interference. The desired and interference multipath signals are shown by blue dotted and red dashed lines, respectively. In a profoundly dense urban communication scenario, the vicinity of both the ends of communication links usually constitutes rich scattering volume. The behavior of the scattering phenomenon in such environments is usually characterized as clustered in spatial domain [6], [39]. The typical composition of angular profiles perceived in such scattering scenarios for both desired and interference channels are also indicated in the figure. The g^{th} cluster of angular domain of interference and desired channel is labeled as $\mathbb{C}_{(\cdot),g}$ where as the cluster of physical scattering points (SP) is labeled as $\mathrm{C}_{(\cdot),g}$, where the $(\cdot)$ takes the label as I and S for interference and desired channel, respectively. The physical clusters can be modeled with different geometrical volumes (i.e. spherical [6] and/or

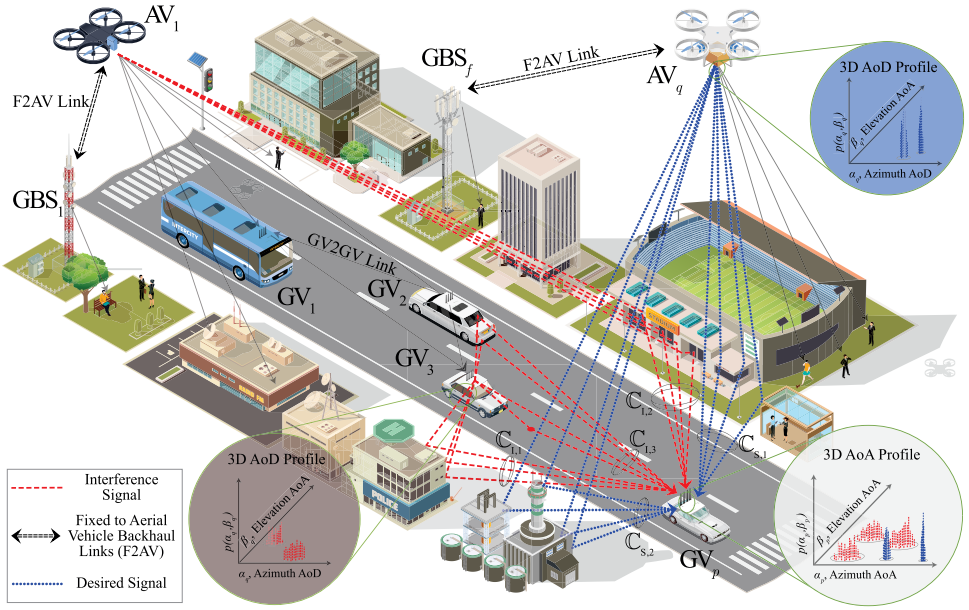

FIGURE 1. Illustration of the considered 3-D volumetric inter-vehicular ultra-dense wireless communication networks.

TABLE 1. Summary of notable literature on angular/spatial domain modeling of interference and desired channels.

Publications	Mobility Scenario	Fading Type	Radio Propagation	Channel Type (Desired and/or Interference)
Waseer et al. [37], 2018	Dual-end 3-D mobility	Rayleigh	3-D space	Independently (Desired or Interference)
Chen et al. [38], 2014	Single-end 2-D mobility	Nakagami-m	2-D plane	Jointly (against SIR)
Nawaz et al. [6], 2017	Single-end 2-D mobility	Nakagami-m	3-D space	Jointly (against SIR)
Du et al. [36], 2019	Single-end 3-D mobility	Nakagami-m	3-D space	Jointly (against SIR)
Proposed Work	**Dual-end 3-D mobility**	**Nakagami-m**	**3-D space**	**Jointly (against SIR)**

elliptical [37] etc.) depending upon the physical composition of the clusters.

The geometric composition drawn from the considered 3-D volumetric inter-vehicular HetNets is depicted in Fig. 2. The composition of scattering clusters in the proposed framework is represented as spherical volumes with different radii and spatial positions in the illuminated 3-D spatial region, where the SP in each cluster are taken as uniformly distributed. Moreover, the scattering clusters are modeled as non-overlapping. The proposed work is generalized in the context of the altitude of the vehicular nodes, while we have illustrated and focused mostly on the interesting emerging scenario of AV2GV communication (e.g. UAV BSs serving ground vehicular user nodes). The coordinates of a certain node (e.g. p^{th} node) at a certain time instant are represented by (x_p, y_p, z_p). For the case illustrated in Fig. 2, the desired AV node's coordinates are taken as $x_p = 0$, $y_p = 0$, and $z_p = h_{\text{AV}}$. The azimuth AoA, elevation AoA, azimuth AoD and elevation AoD for each multipath in a desired or interference channel between p^{th} GV and q^{th} AV are represented as α_p, β_p, α_q, and β_q, respectively. SP are taken as lossless omnidirectional reradiating sources with equal scattering coefficients and uniform random phases. The scattering clusters for desired or interference channel can be taken as common or independent depending upon the spatial positions and visible regions of the desired and interfering sources. Moreover single bounce scattering signals are assumed. The length of a certain multipath constitute the delay of the path i.e. $\tau = \frac{\ell_q + \ell_p}{c}$, where c is the speed of light. In Fig. 2, $\{\vartheta_{v_p}, \vartheta_{v_q}\}$ and $\{\varphi_{v_p}, \varphi_{v_q}\}$ indicate the directions of motion of communicating nodes (i.e., p and q) in azimuth and elevation planes, respectively.

A. DELAY AND DIRECTIONAL SPECTRUM

The independent channel response of desired or interference channels as a function of delay and 3-D directional parameters can be written as given in [6], as follows,

$$\begin{aligned} h_{(\cdot)}(\tau, \alpha_p, \beta_p, \alpha_q, \beta_q) &= \sum_{b=1}^{B} \sqrt{P_\circ} l_b^{\frac{-k_{\text{PL}}}{2}} \hat{\kappa}_b \exp(j\theta_b) \delta(\tau - \tau_b) \delta(\alpha_p - \alpha_{p,b}) \\ &\quad \times \delta(\beta_p - \beta_{p,b}) \delta(\alpha_q - \alpha_{q,b}) \delta(\beta_p - \beta_{p,b}), \end{aligned} \tag{1}$$

where $\sqrt{P_\circ} l_b^{\frac{-k_{\text{PL}}}{2}} \hat{\kappa}_b \exp(j\theta_b)$ is the complex gain of the b^{th} path, $P_\circ$ is the power measured at 1m distance from the

TABLE 2. Definition of proposed model parameters.

S.N.	Parameter	Definition	S.N.	Parameter	Definition
1	AV_q	Label for q^{th} AV	10	$\ell_{(\cdot)}$	3-D distance between a scattering point and vehicular node
2	GV_p	Label for p^{th} GV	11	$\ell'_{(\cdot)}$	Horizontal distance between a scattering point and vehicular node
3	$\mathrm{C}_{\mathrm{S},(\cdot)}$	Cluster of physical scattering points constituting desired channel	12	α_p	Azimuth AoA
4	$\mathrm{C}_{\mathrm{I},(\cdot)}$	Cluster of physical scattering points constituting interference channel	13	α_q	Elevation AoA
5	$\mathbb{C}_{\mathrm{S},(\cdot)}$	Cluster label in angular domain for desired channel	14	β_p	Azimuth AoD
6	$\mathbb{C}_{\mathrm{I},(\cdot)}$	Cluster label in angular domain for interference channel	15	β_q	Elevation AoD
7	d_{LoS}	3-D LoS distance between AV and GV	16	$v_{(\cdot)}$	Direction of motion of vehicles
8	d'_{LoS}	Horizontal LoS distance between AV and GV	17	$\vartheta_{v_{(\cdot)}}$	Azimuth direction of motion of vehicles
9	l_g	Radius of g^{th} cluster	18	$\varphi_{v_{(\cdot)}}$	Elevation direction of motion of vehicles

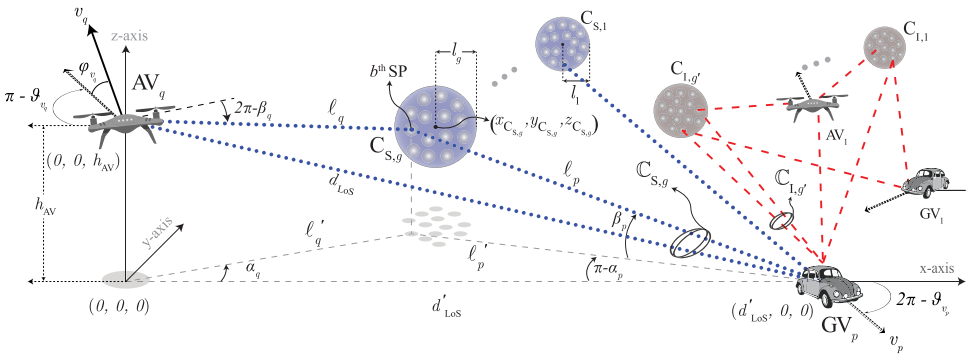

FIGURE 2. Geometric configuration of the proposed system model for interference and desired channels between vehicular (aerial and/or ground) nodes.

source, $\hat{\kappa}_b \exp(j\theta_b)$, and k_{PL} indicate the complex path coefficient and path-loss exponent. The lowest received power ($P_{\min}$) is associated to the path with longest path-length (i.e., $l_{\max}$), which can be related as $l_{\max} = (P_\circ/P_{\min})^{1/k_{\mathrm{PL}}}$. Subsequently, the delay of the longest path can be found as, $\tau_{\max} = l_{\max}/c$. The phase-shift and gain associated to a certain multipath are represented by θ_b and $\hat{\kappa}_b$, respectively, which can be modelled as independent and identically distributed (i.i.d). An empirical study based node's height-dependant path-loss model is proposed in [40], [41], where the range of path-loss exponent to be considered for different nodes heights (between 1.5m and 120m) is provided. In [42], [43], measurement-based path-loss models for V2V communications are presented for different propagation environments (e.g., rural, suburban, urban, and highway). These models can help in choosing an appropriate value for k_{PL} for different altitude levels of the considered AV nodes for different propagation environments. The joint delay directional spectrum (DDS) for independently defining the desired and interference channels can be written as,

$$\begin{aligned}\Xi_{(\cdot)\text{-DDS}}(\tau, \alpha_p, \beta_p, \alpha_q, \beta_q) &= \sum_{b=1}^{B} |h_{(\cdot),b}|^2 \delta(\tau - \tau_b)\delta(\alpha_p - \alpha_{p,b}) \\ &\times \delta(\beta_p - \beta_{p,b})\delta(\alpha_q - \alpha_{q,b})\delta(\beta_p - \beta_{p,b}), \end{aligned} \tag{2}$$

where $h_{(\cdot),b} = \sqrt{P_\circ} l_b^{\frac{-k_{\mathrm{PL}}}{2}} \hat{\kappa}_b \exp(j\theta_b)$ as stated before. By integrating (2) with respect to delay over its appropriate limits (i.e. $\Xi_{(\cdot)\text{-DiS}} = \int_\tau \Xi_{(\cdot)\text{-DDS}} \mathrm{d}\tau$), the directional spectrum (DiS) in 3-D propagation context can be given by,

$$\begin{aligned}&\Xi_{(\cdot)\text{-DiS}}(\alpha_p, \beta_p, \alpha_q, \beta_q) \\ &= \int_\tau \mathbb{E}\Big[\Xi_{(\cdot)\text{-DiS}}(\tau, \alpha_p, \beta_p, \alpha_q, \beta_q)\Big]\mathrm{d}\tau, \\ &\propto \int_\tau \mathbb{E}\Big[|h_{(\cdot),b}|^2|_{\tau,\alpha_p,\beta_p,\alpha_q,\beta_q}\Big] \\ &\quad \times f_{\tau,\alpha_p,\beta_p,\alpha_q,\beta_q}(\tau, \alpha_p, \beta_p, \alpha_q, \beta_q)\mathrm{d}\tau, \\ &\propto f_{\alpha_p,\beta_p,\alpha_q,\beta_q}(\alpha_p, \beta_p, \alpha_q, \beta_q) \\ &\quad \times \int_\tau \mathbb{E}\Big[|h_{(\cdot),b}|^2|_{\tau,\alpha_p,\beta_p,\alpha_q,\beta_q}\Big]\mathrm{d}\tau, \end{aligned} \tag{3}$$

where $\mathbb{E}[\cdot]$ represents the statistical expectation and $f_{\tau,\alpha_p,\beta_p,\alpha_q,\beta_q}(\tau, \alpha_p, \beta_p, \alpha_q, \beta_q)$ represents the joint probability distribution function (jPDF) of ToA, 3-D AoA, and 3-D AoD. Subsequently, the reduced function $f_{\alpha_p,\beta_p,\alpha_q,\beta_q}(\alpha_p, \beta_p, \alpha_q, \beta_q)$ represents the jPDF of 3-D AoA and 3-D

AoD. The azimuth spectrum (AS) can be obtained by,

$$\begin{aligned}\Xi_{(\cdot)\text{-AS}}(\alpha_A) &= \int_{\beta_q}\int_{\beta_p}\int_{\alpha_{\hat{A}}} \mathbb{E}\Big[\Xi_{(\cdot)\text{-DiS}}(\alpha_p,\beta_p,\alpha_q,\beta_q)\Big]\mathrm{d}\alpha_{\hat{A}}\mathrm{d}\beta_p\mathrm{d}\beta_q,\\ &\propto \int_{\beta_q}\int_{\beta_p}\int_{\alpha_{\hat{A}}} \mathbb{E}\Big[|h_{(\cdot),b}|^2|_{\alpha_p,\beta_p,\alpha_q,\beta_q}\Big]\\ &\quad\times f_{\alpha_p,\beta_p,\alpha_q,\beta_q}(\alpha_p,\beta_p,\alpha_q,\beta_q)\mathrm{d}\alpha_{\hat{A}}\mathrm{d}\beta_p\mathrm{d}\beta_q, \end{aligned} \tag{4}$$

and elevation spectrum (ES) as follows,

$$\begin{aligned}\Xi_{(\cdot)\text{-ES}}(\beta_A) &= \int_{\alpha_q}\int_{\alpha_p}\int_{\beta_{\hat{A}}} \mathbb{E}\Big[\Xi_{(\cdot)\text{-DiS}}(\alpha_p,\beta_p,\alpha_q,\beta_q)\Big]\mathrm{d}\beta_{\hat{A}}\mathrm{d}\alpha_p\mathrm{d}\alpha_q,\\ &\propto \int_{\alpha_q}\int_{\alpha_p}\int_{\beta_{\hat{A}}} \mathbb{E}\Big[|h_{(\cdot),b}|^2|_{\alpha_p,\beta_p,\alpha_q,\beta_q}\Big]\\ &\quad\times f_{\alpha_p,\beta_p,\alpha_q,\beta_q}(\alpha_p,\beta_p,\alpha_q,\beta_q)\mathrm{d}\beta_{\hat{A}}\mathrm{d}\alpha_p\mathrm{d}\alpha_q, \end{aligned} \tag{5}$$

where the $A, \hat{A} \in [p, q]$. If A takes the value as p then the value of $\hat{A}$ must be taken as q and vice versa.

B. GEOMETRIC COMPOSITION OF SCATTERING CLUSTERS AND ANGULAR STATISTICS

For evaluating the analytical expressions derived for second-order fading statistics of the desired and interference channels, a multi-cluster scattering scenario is considered. The mobility context of communicating nodes can be considered restricted to within a certain local-region (or observation span) in which the channel statistics can be assumed as stationary. Such local-region (or observation-span) can be defined as a region along the mobility of nodes in which the channel statistics remain 50% or more correlated. The scale of such stationary local-region depends on the mobility conditions (direction and velocity of node's motion) and nature of considered propagation environment. For different V2V radio propagation environments, both stationary and non-stationary spatial channel models have been proposed in the literature, see e.g., [44] and [45], respectively. In the considered 3-D ellipsoidal channel model, the boundary of the effective scattering region (ESR) is defined as limited by a predefined minimum-power threshold level. This threshold determines the length of the longest effective multipath. By exploiting the geometric property of ellipsoids that the composite length of the two lines drawn from two different foci points of an ellipsoid to a point on it surface remains the same for all the points on the surface of the ellipsoid, the boundary of ESR can be drawn as ellipsoidal shaped [46]. This bounding ellipsoid contains the communicating vehicular nodes fixed on its foci points, while the ellipsoid moves and transforms along the mobility of the nodes. Due to the motion of nodes the dimensions of the bounding ellipsoid changes in order to ensure the length of the lowest-power (longest) multipath remains constant. The time-evolution in the ESR for the considered system model is shown in Fig. 3, where three consecutive time-snaps are illustrated. The definition of fully illuminated, partially illuminated and inactive scattering clusters is also labeled in the figure. Given the initial coordinates (position) of the communicating nodes and the direction and velocity of motion of the nodes, the expression for time-evolving bounding ellipsoid can be written as given in (6).

The axes of the time-evolving bounding ellipsoid can be expressed as $a_{\max}(t) = l_{\max}/2$ and $b_{\max}(t) = c_{\max}(t) = \frac{1}{2}\sqrt{l_{\max}^2 - d_{\text{LoS}}^2(t)}$. The shift parameters (i.e.,g the coordinates of the origin of the bounding ellipsoid $(x_\circ(t), y_\circ(t), z_\circ(t))$) and rotation parameters (α_{LoS} and β_{LoS}) can be expressed as follows,

$$\alpha_{\text{LoS}} = \arctan\left(\left|\frac{y_p(t)-y_q(t)}{x_p(t)-x_q(t)}\right|\right),$$

$$\beta_{\text{LoS}} = \arctan\left(\frac{|z_p(t)-z_q(t)|}{\sqrt{(x_p(t)-x_q(t))^2+(x_p(t)-x_q(t))^2}}\right),$$

$$x_\circ(t) = \frac{(x_p(t)+x_q(t))}{2},$$

$$y_\circ(t) = \frac{(y_p(t)+y_q(t))}{2}, \text{ and}$$

$$z_\circ(t) = \frac{(z_p(t)+z_q(t))}{2}.$$

The coordinates of p^{th} and q^{th} mobile nodes at any time instant t can be computed by using the coordinates of their initial position, direction of motion in horizontal and vertical axes, and velocity of motion. For example, the coordinates of p^{th} node are expressed as follows,

$$\begin{aligned} x_p(t) &= x_p(t_\circ) + v_p\ \Delta t\ \cos\beta_p\cos\alpha_p,\\ y_p(t) &= y_p(t_\circ) + v_p\ \Delta t\ \cos\beta_p\sin\alpha_p, \text{ and}\\ x_p(t) &= x_p(t_\circ) + v_p\ \Delta t\ \sin\beta_p, \end{aligned}$$

where $\Delta t = t - t_\circ$, where t is current time instant and $t_\circ$ is the initial time instant. This time difference between current and initial positions can also be modeled as discretely sampled; i.e., $\Delta t = nT_s$, where n indicates the sample index and T_s represents the sample interval.

At a given time instant, only the clusters that lie within the bounding ellipsoid are considered as the effective scattering clusters. The scattering clusters can be modeled as spherical shaped with each cluster having different radius and spatial position. A spherical shaped scattering cluster (e.g., g^{th} cluster) can be expressed as,

$$\frac{(x_{\text{IP}}-x_{C_{(\cdot),g}})^2}{l_g^2} + \frac{(y_{\text{IP}}-y_{C_{(\cdot),g}})^2}{l_g^2} + \frac{(z_{\text{IP}}-z_{C_{(\cdot),g}})^2}{l_g^2} \le 1, \tag{7}$$

where l_g represents the radius of g^{th}, and $g \in \{1, 2, \ldots, G\}$. The ESR is thus defined as the intersection region of the bound ellipsoid and the scattering clusters, i.e., (6) $\cap$ (7). If the intersection point of the lines drawn along the given direction of departure (α_q, β_q) and direction of arrival (α_p, β_p) lies within the overlapping region of bounding ellipsoid (as

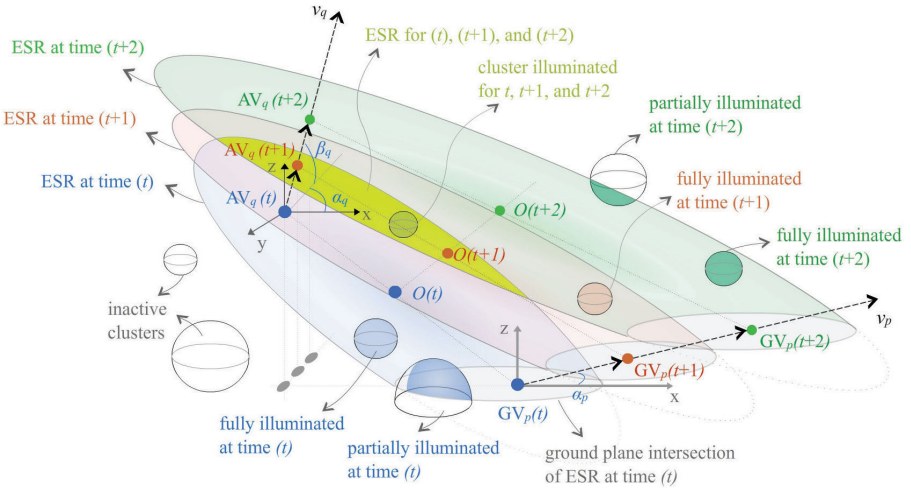

FIGURE 3. Illustration of the transformations in the composition of ESR for a certain channel (i.e., desired or interference) caused by the mobility of communicating nodes.

defined by (6)), as shown at the bottom of the this page and any scattering cluster (as defined by (7)), then the probability of occurrence of multipath is V_b/V_{ESR}. The parameter V_b represents the volume of region of intersection of two cones originated from the transmitter and receiver sides as oriented along the direction of departure and arrival, while V_{ESR} represents the total volume of effective scattering region. For achieving mathematical simplicity in the normalization of probability density function (PDF), V_b may be taken as 1. The jPDF of AoA and AoD can be written as follows,

$$f_{(\cdot)}(\alpha_p, \beta_p, \alpha_q, \beta_q) = \begin{cases} \dfrac{1}{V_{\text{ESR}}}; & (x_{\text{IP}}, y_{\text{IP}}, z_{\text{IP}}) \in \text{ESR} \\ 0; & \text{otherwise.} \end{cases} \tag{8}$$

The coordinates of the intersection points (IP) for a given direction of departure and direction of arrival can be evaluated as,

$$x_{\text{IP}} = \frac{d'_{\text{LoS}} \cos\alpha_q \sin\alpha_p}{\sin(\pi - \alpha_q - \alpha_p)}, \tag{9}$$

$$y_{\text{IP}} = \frac{d'_{\text{LoS}} \sin\alpha_q \sin\alpha_p}{\sin(\pi - \alpha_q - \alpha_p)}, \tag{10}$$

and

$$z_{\text{IP}} = \frac{d'_{\text{LoS}} \sin\alpha_q \sin\beta_p}{\sin(\pi - \alpha_q - \alpha_p)\cos\beta_p}. \tag{11}$$

The random fluctuations that occur in the received signal can be expressed as a function of directional statistics of desired and interference channels. The joint angular power distribution (APD) of a certain channel (desired or interference) for the considered system model can be defined as,

$$p(\alpha_p, \beta_p, \alpha_q, \beta_q) = f(\alpha_p, \beta_p, \alpha_q, \beta_q) \times G(\alpha_p, \beta_p, \alpha_q, \beta_q), \tag{12}$$

where $G(.,.,.,.)$ represents the combined antenna-array beam pattern of transmitter and receiver sides. As the transmitter and receiver side antenna beam patterns are independent of each other, therefore, it can be expressed as $G(\alpha_p, \beta_p, \alpha_q, \beta_q) = G(\alpha_p, \beta_p)G(\alpha_q, \beta_q))$. These beam patterns can be modeled as 3-D Gaussian shaped [47] or any other shape depending upon the antenna element's shape and configuration. In the joint APD presented in (12), the joint gain of antenna-arrays at transmiter and receiver sides is a dominating factor when compared to the angular profile resulted purely from the radio propagation environment. Therefore, in order to purely investigate the impact of physical environment, the contributions caused by the antenna-array gain are ignored in this work. In this context, the antenna-array gain parameter $G(\alpha_p, \beta_p, \alpha_q, \beta_q)$ is taken as equal to 1. The function $f(.,.,.,.)$ represents jPDF of 3-D AoA and 3-D AoD, which is described in equation (8) for a typical multi-cluster scattering environment. The total power from the APD function can be obtained as

$$\frac{\big((x_p(t) - x_\circ(t))\cos\alpha_{\text{LoS}}(t)\cos\beta_{\text{LoS}}(t) + (y_p(t) - y_\circ(t))\sin\alpha_{\text{LoS}}(t)\cos\beta_{\text{LoS}}(t) + (z_p(t) - z_\circ(t))\sin\beta_{\text{LoS}}(t)\big)^2}{a^2_{\max}(t)}$$
$$+\frac{\big((y_p(t) - y_\circ(t))\cos\alpha_{\text{LoS}}(t) - (x_p(t) - x_\circ(t))\sin\alpha_{\text{LoS}}(t)\big)^2}{b^2_{\max}(t)}$$
$$+\frac{\big((z_p(t) - z_\circ(t))\cos\beta_{\text{LoS}}(t) - (y_p(t) - y_\circ(t))\sin\alpha_{\text{LoS}}(t)\sin\beta_{\text{LoS}}(t) - (x_p(t) - x_\circ(t))\cos\alpha_{\text{LoS}}(t)\sin\beta_{\text{LoS}}(t)\big)^2}{c^2_{\max}(t)} \leq 1. \tag{6}$$

$\int\int\int\int_{E} p(\alpha_p, \beta_p, \alpha_q, \beta_q)\mathrm{d}e = P_{\mathrm{T}}$. The azimuth AoA and AoD (i.e. α_p and α_q) are bounded by 0 to 2π, while elevation AoA and AoD (i.e. β_p and β_q) bounded by $-\frac{\pi}{2}$ to $+\frac{\pi}{2}$. E shows the unit sphere where de is an elemental part of the unit sphere in 3-D space.

III. SECOND-ORDER FADING STATISTICS OF DESIRED AND INTERFERENCE CHANNELS

The jPDF of 3-D AoA and 3-D AoD can be used to compute complex double spherical harmonics coefficients, $S_{v,w}^{a,u}$. The important harmonics for quantification of 3-D angular spread/deviation, as given by [37], in V2V communication context can be obtained as follows,

$$S_{v,w}^{a,u} = \int_{-\pi}^{\pi}\int_{-\frac{\pi}{2}}^{\frac{\pi}{2}}\int_{-\pi}^{\pi}\int_{-\frac{\pi}{2}}^{\frac{\pi}{2}} \Big\{ f(\alpha_p, \beta_p, \alpha_q, \beta_q) \times Y_{v,w}^{a,u*} \Big\} \mathrm{d}\beta_p \mathrm{d}\alpha_p \mathrm{d}\beta_q \mathrm{d}\alpha_q, \quad (13)$$

where the simplified parameters of double spherical harmonics $Y_{v,w}^{a,u}$ are later utilized in the definition of second-order fading statistics, are listed as follows,

$$\begin{aligned}
Y_{0,0}^{0,0} &= 1,\ Y_{1,0}^{0,0} = \sin\beta_p,\ Y_{0,1}^{0,0} = \sin\beta_q,\\
Y_{1,1}^{1,0} &= \cos\beta_p \exp(j\alpha_p)\sin\beta_q,\\
Y_{1,1}^{1,1} &= \cos\beta_p \cos\beta_q \exp(j(\alpha_p + \alpha_q)),\\
Y_{1,1}^{1,-1} &= \cos\beta_p \cos\beta_q \exp(j(\alpha_p - \alpha_q)),\\
Y_{1,0}^{1,0} &= \cos\beta_p \exp(j\alpha_p, Y_{1,0}^{0,1}) = \cos\beta_q \exp(j\alpha_q),\\
Y_{2,0}^{0,0} &= \left(2\sin^2\beta_p - \frac{2}{3}\right),\quad Y_{0,2}^{0,0} = \left(2\sin^2\beta_q - \frac{2}{3}\right),\\
Y_{0,2}^{0,1} &= \sin 2\beta_q \exp(j\alpha_q, Y_{0,1}^{0,1}) = \cos\beta_q \exp(j\alpha_q),\\
Y_{0,1}^{0,-1} &= \cos\beta_q \exp(-j\alpha_q, Y_{1,1}^{0,0}) = \sin\beta_p \sin\beta_q,\\
Y_{2,0}^{1,0} &= \sin 2\beta_p \exp(j\alpha_p, Y_{2,0}^{2,0}) = \cos^2\beta_p \exp(j2\alpha_p),\\
Y_{1,1}^{0,1} &= \cos\beta_q \exp(j\alpha_q \sin\beta_p, Y_{0,2}^{0,2}) = \cos^2\beta_q \exp(j2\alpha_q).
\end{aligned} \quad (14)$$

A. ANGULAR SPREAD QUANTIFICATION

The integration of the multi-antenna systems with 3-D volumetric vehicular communications provides the capability of manipulations in spatial domain of the channel. For example, directional beams can help in reducing the angular spread through spatial filtering of multipaths, which further reduces the Doppler spread and increases the channel coherent time. Quantification of angular spread in 3-D space is of high significance. There are various quantifiers proposed in the literature, see e.g., [6], [10], [34], [37], [48]. In this study, we have utilized the quantifiers proposed in [37] for quantification of the energy dispersion in 3-D space in an inter-vehicular context.

Table 3 summarizes the angular spread quantifiers (also referred to as multipath shape factors) proposed in [37]. The values increasing from 0 to 1 for Angular Spread represent the increase in overall joint 3-D spatial spread, where the value 1 shows the maximum spread. In Elevational Constriction −0.5 demonstrates the probability of the received signal along a single elevational cone; whereas signals coming from two opposite elevational angles at one azimuthal angle give a value of 1. In 45°-Inclined Constriction values range from 0 to 1. Value of 0 represents a symmetric nature of the received signal along the vertical and/or horizontal axis; 1 demonstrates the arrival of the signal from two vertical directions from mirror-symmetric headings in respect to a 45°-inclined axis. Value of Azimuthal Constriction also ranges from 0 to 1. Value of 1 represents signals received from two different path having same elevation; value of 0 indicates no clear bias. Azimuth of Maximum Fading at 45° Elevation gives the azimuthal angle which causes most fading at an elevation of 45°. Azimuth of Maximum Fading at 0° Elevation, Azimuth of Jointly Maximum Fading at 0° Elevation and Azimuth of Jointly Maximum Cross-Angular Fading give the accurate physical direction of the maximum fading. In Joint Elevational Constriction, Positive and Negative Joint Azimuthal Constriction and Joint Cross-Angular Constriction value of 1 demonstrates the convergence of signals about precisely two paths, while 0 indicates no clear bias.

B. FADING RATE VARIANCE OF COMPLEX ENVELOPE

The mobility conditions (direction and velocity) of the vehicular nodes and the spatial characteristics of radio propagation environment determine the channel fading behaviour. The essential stochastic processes for studying the wireless channel fading characteristics are the received signal envelope and power [49]. The rate of fluctuations in these variables can be measured in terms of their variance or standard deviation. The expected value of the mean-square of the process represents fading rate variance. Fading rate variance in a 2-D radio propagation environment in a F2V communication context is derived in [49]. For a V2V communication context in 3-D radio propagation environment, the fading rate variance (for independent interference and desired channels) derived in [37], is given in (15), as shown at the bottom of the next page.

This fading rate variance of independent interference and desired channels is further utilized to determine the joint second-order fading statistics of the interference and desired channels in the following subsections.

C. LEVEL CROSSING RATE (LCR)

The mathematical expression of LCR can be written as follows,

$$N_R = \int_0^{\infty} \dot{r} f_{R\dot{R}}(R, \dot{r})\mathrm{d}\dot{r}, \quad (16)$$

where R, $\dot{r}$, and $f_{R\dot{R}}(R, \dot{r})$ represent the threshold-level being observed, derivative of the envelope along time, and jPDF of envelope and its time derivative, respectively.

Nakagami-m distribution to model the channel fading behaviour is considered as notable [50] for its ability to

TABLE 3. 3-D multipath shape factors for V2V communications [37].

Quantifier	Expression	Range
Angular Spread	$\Upsilon_{p_{(\cdot)}} = \sqrt{1 - \frac{S_{1,0}^{0,0^2} + \lvert S_{1,0}^{1,0}\rvert^2}{S_{0,0}^{0,0^2}}}$, $\Upsilon_{q_{(\cdot)}} = \sqrt{1 - \frac{S_{1,0}^{1,0} + \lvert S_{0,1}^{0,1}\rvert^2}{S_{0,0}^{0,0^2}}}$.	$0 \sim 1$
Elevational Constriction	$\xi_{p_{(\cdot)}} = \frac{\frac{3}{2}S_{0,2}^{0,0}S_{0,0}^{0,0} - \left(S_{1,0}^{0,0^2} - \frac{1}{2}\lvert S_{1,0}^{1,0}\rvert^2\right)}{S_{1,0}^{1,0} - \left(S_{1,0}^{0,0^2} - \lvert S_{1,0}^{1,0}\rvert^2\right)}$, $\xi_{q_{(\cdot)}} = \frac{\frac{3}{2}S_{2,0}^{0,0}S_{0,0}^{0,0} - \left(S_{1,0}^{0,0^2} - \frac{1}{2}\lvert S_{1,0}^{1,0}\rvert^2\right)}{S_{0,0}^{0,0^2} - \left(S_{1,0}^{0,0^2} - \lvert S_{1,0}^{1,0}\rvert^2\right)}$.	$-0.5 \sim 1$
45° - Inclined Constriction	$\chi_{p_{(\cdot)}} = \frac{2\lvert S_{2,0}^{1,0}S_{0,0}^{0,0} - S_{1,0}^{0,0}S_{1,0}^{1,0}\rvert}{S_{0,0}^{0,0^2} - \left(S_{1,0}^{1,0} + \lvert S_{1,0}^{1,0}\rvert^2\right)}$, $\chi_{q_{(\cdot)}} = \frac{2\lvert S_{0,2}^{1,0}S_{0,0}^{0,0} - S_{1,0}^{0,0}S_{1,0}^{1,0}\rvert}{S_{0,0}^{0,0^2} - \left(S_{1,0}^{0,0^2} - \lvert S_{1,0}^{1,0}\rvert^2\right)}$.	$0 \sim 1$
Azimuthal Constriction	$\zeta_{p_{(\cdot)}} = \frac{\lvert S_{2,0}^{2,0}S_{0,0}^{0,0} - S_{1,0}^{1,0^2}\rvert}{S_{0,0}^{0,0^2} - \left(S_{1,0}^{0,0^2} - \lvert S_{1,0}^{1,0}\rvert^2\right)}$, $\zeta_{q_{(\cdot)}} = \frac{\lvert S_{0,2}^{0,2}S_{0,0}^{0,0} - S_{1,0}^{1,0^2}\rvert}{S_{0,0}^{0,0^2} - \left(S_{1,0}^{0,0^2} - \lvert S_{1,0}^{1,0}\rvert^2\right)}$.	$0 \sim 1$
Azimuth of Maximum Fading at 45° Elevation	$\phi^{\max}_{\beta_p 45_{(\cdot)}} = \arg\left\{S_{2,0}^{1,0}S_{0,0}^{0,0} - S_{1,0}^{0,0}S_{1,0}^{1,0}\right\}$, $\phi^{\max}_{\beta_q 45_{(\cdot)}} = \arg\left\{S_{0,2}^{0,1}S_{0,0}^{0,0} - S_{1,0}^{0,0}S_{1,0}^{1,0}\right\}$.	$-\pi \sim \pi$
Azimuth of Maximum Fading at 0° Elevation	$\phi^{\max}_{\beta_p 0_{(\cdot)}} = \frac{1}{2}\arg\left\{S_{0,2}^{2,0}S_{0,0}^{0,0} - S_{1,0}^{1,0^2}\right\}$, $\phi^{\max}_{\beta_q 0_{(\cdot)}} = \frac{1}{2}\arg\left\{S_{0,2}^{2,0}S_{0,0}^{0,0} - S_{1,0}^{1,0^2}\right\}$.	$-\pi \sim \pi$
Azimuth of Jointly Maximum Fading at 0° Elevation	$\phi^{\max}_{pq0_{(\cdot)}} + \phi^{\max}_{qp0_{(\cdot)}} = \arg\left\{S_{0,0}^{0,0}S_{1,1}^{1,1} - S_{1,0}^{1,0}S_{0,1}^{0,1}\right\}$, $\phi^{\max}_{pq0_{(\cdot)}} - \phi^{\max}_{qp0_{(\cdot)}} = \arg\left\{S_{0,0}^{0,0}S_{1,1}^{1,-1} - S_{1,0}^{1,0}S_{0,1}^{0,-1}\right\}$.	$-\pi \sim \pi$
Azimuth of Jointly Maximum Cross-Angular Fading	$\phi^{\max}_{p/\beta_q{}_{(\cdot)}} = \arg\left\{S_{0,0}^{0,0}S_{1,1}^{1,0} - S_{1,0}^{1,0}S_{0,1}^{0,0}\right\}$, $\phi^{\max}_{q/\beta_p{}_{(\cdot)}} = \arg\left\{S_{0,0}^{0,0}S_{1,1}^{0,1} - S_{1,0}^{0,0}S_{0,1}^{0,1}\right\}$.	$-\pi \sim \pi$
Joint Elevational Constriction	$\Xi_{(\cdot)} = \frac{2\left(S_{1,1}^{0,0} - S_{1,0}^{0,0} - S_{0,1}^{0,0}\right)}{2S_{1,1}^{0,0^2} - \left(S_{1,0}^{0,0^2} + S_{0,1}^{0,0^2} + \lvert S_{1,0}^{1,0}\rvert^2 + \lvert S_{0,1}^{0,1}\rvert^2\right)}$.	$0 \sim 1$
Positive and Negative Joint Azimuthal Constriction	$\Delta_{+_{(\cdot)}} = \frac{2\lvert S_{0,0}^{0,0}S_{1,1}^{1,-1} - S_{1,0}^{1,0} - S_{0,1}^{0,-1}\rvert}{2S_{1,1}^{0,0^2} - \left(S_{1,0}^{0,0^2} + S_{0,1}^{0,0^2} + \lvert S_{1,0}^{1,0}\rvert^2 + \lvert S_{0,1}^{0,1}\rvert^2\right)}$, $\Delta_{-_{(\cdot)}} = \frac{2\lvert S_{0,0}^{0,0}S_{1,1}^{1,1} - S_{1,0}^{1,0} - S_{0,1}^{0,1}\rvert}{2S_{1,1}^{0,0^2} - \left(S_{1,0}^{0,0^2} + S_{0,1}^{0,0^2} + \lvert S_{1,0}^{1,0}\rvert^2 + \lvert S_{0,1}^{0,1}\rvert^2\right)}$.	$0 \sim 1$
Joint Cross-Angular Constriction	$\kappa^q_{p_{(\cdot)}} = \frac{2\lvert S_{0,0}^{0,0}S_{1,1}^{1,0} - S_{1,0}^{1,0} - S_{0,1}^{0,0}\rvert}{2S_{1,1}^{0,0^2} - \left(S_{1,0}^{0,0^2} + S_{0,1}^{0,0^2} + \lvert S_{1,0}^{1,0}\rvert^2 + \lvert S_{0,1}^{0,1}\rvert^2\right)}$, $\kappa^p_{q_{(\cdot)}} = \frac{2\lvert S_{0,0}^{0,0}S_{1,1}^{0,1} - S_{0,1}^{0,1} - S_{1,0}^{0,0}\rvert}{2S_{1,1}^{0,0^2} - \left(S_{1,0}^{0,0^2} + S_{0,1}^{0,0^2} + \lvert S_{1,0}^{1,0}\rvert^2 + \lvert S_{0,1}^{0,1}\rvert^2\right)}$.	$0 \sim 1$

represent Rayleigh, Exponential, and Weibull distributions as its special cases. Moreover, despite the behaviour of Rician and Nakagami-*m* distributions is approximately equivalent, especially around the mean value, Nakagami-*m* distribution

$$\begin{aligned}\sigma^2_{\tilde{V}_{(\cdot)}} = \frac{\omega^2_{\max} P_{\mathrm{T}(\cdot)}}{3}\Bigg\{&\Upsilon^2_{p_{(\cdot)}}\Bigg(1 + \frac{3}{2}\Bigg(\xi_{p(\cdot)}\left(2\sin^2\varphi_{v_p} - \frac{2}{3}\right) + \chi_{p_{(\cdot)}}\sin\left(2\varphi_{v_p}\right)\cos\left(\vartheta_{v_p} - \phi^{\max}_{\beta_p 45_{(\cdot)}}\right)\\ &+\zeta_{p_{(\cdot)}}\cos^2\varphi_{v_p} \times \cos\left(2\left(\vartheta_{v_p} - \phi^{\max}_{\beta_p 0_{(\cdot)}}\right)\right)\Bigg)\Bigg) + \Upsilon^2_{q_{(\cdot)}}\Bigg(1 + \frac{3}{2}\Bigg(\xi_{q(\cdot)}\left(2\sin^2\varphi_{v_q} - \frac{2}{3}\right) + \chi_{q_{(\cdot)}}\sin 2\varphi_{v_q}\\ &\times\cos\left(\vartheta_{v_q} - \phi^{\max}_{\beta_q 45_{(\cdot)}}\right) + \zeta_{q_{(\cdot)}}\cos^2\varphi_{v_q}\cos\left(2\left(\vartheta_{v_q} - \phi^{\max}_{\beta_q 0_{(\cdot)}}\right)\right)\Bigg)\Bigg) + \left(\Upsilon^2_{p_{(\cdot)}} + \Upsilon^2_{q_{(\cdot)}}\right)\Bigg(\Xi_{(\cdot)}\sin\varphi_{v_p}\sin\varphi_{v_q}\\ &+\Delta_{+(\cdot)}\cos\left(\vartheta_{v_p} - \vartheta_{v_q} - \left(\phi^{\max}_{pq0_{(\cdot)}} - \phi^{\max}_{qp0_{(\cdot)}}\right)\right) + \Delta_{-(\cdot)}\cos\left(\vartheta_{v_p} + \vartheta_{v_q} - \left(\phi^{\max}_{pq0_{(\cdot)}} + \phi^{\max}_{qp0_{(\cdot)}}\right)\right) + \kappa^q_{p_{(\cdot)}}\\ &\times\cos\left(\vartheta_{v_p} - \phi^{\max}_{p/\beta_q{}_{(\cdot)}}\right) \times \sin\varphi_{v_q} + \kappa^p_{q_{(\cdot)}}\cos\left(\vartheta_{v_q} - \phi^{\max}_{q/\beta_p{}_{(\cdot)}}\right)\sin\varphi_{v_p}\Bigg)\Bigg\}. \end{aligned} \tag{15}$$

is mathematically more tractable [51]. Considering these aspects, Nakagami-m fading channels are considered this work. The Nakagami-m PDF can be expressed as given by [52], as follows,

$$f_r(r) = \left(\frac{m}{P_{\mathrm{T}}}\right)^m \left(\frac{2}{\Gamma(m)}\right) \times r^{(2m-1)} \exp -\left(\frac{mr^2}{P_{\mathrm{T}}}\right), \quad r \geq 0 \text{ and } m \geq \frac{1}{2}, \tag{17}$$

where $P_{\mathrm{T}} = \mathbb{E}[r^2]$, $\Gamma(\cdot)$ is the Gamma function, and $m = \frac{\mathbb{E}[r^2]}{\mathbb{VAR}[r^2]}$. It should be noted that, in contrast to the instantaneous power distribution, the amplitude distribution of $R(t)$ and its rate of change $\dot{r}(t)$ are statistically independent. Therefore, $f_{R\dot{R}}(R, \dot{r}) = f(R)f(\dot{r})$, where $f(\dot{r})$ represents the PDF of time derivative of the envelope. So, the jPDF of envelope and its time derivative can be written as [53],

$$f_{R\dot{r}}(R, \dot{r}) = \left(\frac{m}{P_{\mathrm{T}}}\right)^m \left(\frac{2}{\Gamma(m)}\right) r^{(2m-1)} \exp\left(\frac{-mr^2}{P_{\mathrm{T}}}\right) \times \sqrt{\frac{4m}{P_{\mathrm{T}}}} \frac{1}{\sqrt{2\pi|\ddot{r}(0)|}} \exp\left(\frac{2m\dot{r}^2}{P_{\mathrm{T}}|\ddot{r}(0)|}\right). \tag{18}$$

An expression for LCR can be obtained by substituting (18) in (16), as given by [53], which is shown as follows,

$$N_{R_{(\cdot)}} = \sigma_{\tilde{\dot{V}}_{(\cdot)}} \left\{ \exp\left(-m_{(\cdot)}\widetilde{R}_{(\cdot)}^2\right) \times \frac{\widetilde{R}_{(\cdot)}^{(2m_{(\cdot)}-1)} m_{(\cdot)}^{(m_{(\cdot)}-1/2)}}{\Gamma(m_{(\cdot)})\sqrt{\pi P_{\mathrm{T}_{(\cdot)}}}} \right\}, \tag{19}$$

where the subscript $(\cdot)$ of $N_{R_{(\cdot)}}$ takes the label as S or I to represent the LCR of desired ($N_{R_{\mathrm{S}}}$) or interference channels ($N_{R_{\mathrm{I}}}$), respectively. The parameter $\widetilde{R}_{(\cdot)}$ represents the normalized threshold level of observation, i.e., $\widetilde{R}_{(\cdot)} = R_{(\cdot)}/P_{\mathrm{T}_{(\cdot)}}$. LCR for both the desired and interference channels can be jointly characterized in terms of SIR (i.e., η). To this end, the joint density function of the desired and interference signals and their derivatives at any spatial position, i.e., $f_{r_{\mathrm{I}},\dot{r}_{\mathrm{I}},r_{\mathrm{S}},\dot{r}_{\mathrm{S}}}(r_{\mathrm{I}}, \dot{r}_{\mathrm{I}}, r_{\mathrm{S}}, \dot{r}_{\mathrm{S}})$, can be utilized. The threshold level for the LCR of SIR (N_{R_η}) is defined as $R_\eta = \frac{r_{\mathrm{S}}^2}{r_{\mathrm{I}}^2}$. When the interference and desired signals are assumed to be independent, then the LCR of SIR for a 3-D propagation environment constituting Nakagami-m fading derived in [38] can be given by,

$$N_{R_\eta} = \int_0^\infty f_{r_{\mathrm{I}}}(r_{\mathrm{I}}) f_{r_{\mathrm{S}}}\left(\sqrt{r_{\mathrm{I}}^2\widetilde{R}_\eta}\right) \mathrm{d}(r_{\mathrm{I}}) \int_{-\infty}^{\infty} \int_{-\infty}^{\dot{r}_{\mathrm{S}}} f_{\dot{r}_{\mathrm{I}}}(\dot{r}_{\mathrm{I}}) \times f_{\dot{r}_{\mathrm{S}}}(\dot{r}_{\mathrm{S}}) \left\{ \frac{\sqrt{\widetilde{R}_\eta}}{\min\left\{\left|\frac{1}{\dot{r}_{\mathrm{I}}}\right|, \left|\frac{\sqrt{\widetilde{R}_\eta}}{\dot{r}_{\mathrm{S}}}\right|\right\}} \right\} \mathrm{d}(\dot{r}_{\mathrm{I}}) \mathrm{d}(\dot{r}_{\mathrm{S}}). \tag{20}$$

The PDF of the time derivative of envelopes $\dot{r}_{\mathrm{S}}$ and $\dot{r}_{\mathrm{I}}$ follows Gaussian distribution with standard deviation of desired and interference signal given by $\sigma_{V_{\mathrm{S}}}/2m_{\mathrm{S}}$ and $\sigma_{V_{\mathrm{I}}}/2m_{\mathrm{I}}$, respectively. The equation for LCR in terms of SIR given in (20) can be further solved for two special cases, which are discussed as follows.

Case I: The first special case represents the case when the rate of fluctuations in the interference signal is much lower than the the rate of fluctuations in the desired signal, i.e., $N_{R_{\mathrm{I}}} \ll N_{R_{\mathrm{S}}}$. The threshold level of observation for SIR can be defined as $\widetilde{R}_\eta = \frac{\widetilde{R}_{\mathrm{S}}^2 P_{\mathrm{T}_{\mathrm{S}}}}{r_{\mathrm{I}}^2}$. Mathematical expression for LCR for this case can be derived as,

$$N_{R_\eta} \cong \int_0^\infty \frac{\left(\frac{\widetilde{R}_\eta r_{\mathrm{I}}^2}{P_{\mathrm{T}_{\mathrm{S}}}}\right)^{m_{\mathrm{S}}-\frac{1}{2}} m_{\mathrm{I}}^{m_{\mathrm{I}}} m_{\mathrm{S}}^{m_{\mathrm{S}}-\frac{1}{2}} r_{\mathrm{I}}^{2m_{\mathrm{I}}-1}}{\Gamma(m_{\mathrm{S}})\Gamma(m_{\mathrm{I}})\sqrt{3}P_{\mathrm{T}_{\mathrm{I}}}^{m_{\mathrm{I}}}} \times \sigma_{\tilde{\dot{V}}_{\mathrm{S}}} \omega_{\max} \sqrt{P_{\mathrm{T}S}} \exp\left(\frac{-r_{\mathrm{I}}^2 P_{\mathrm{T}_{\mathrm{I}}} m_{\mathrm{S}} \widetilde{R}_\eta + m_{\mathrm{I}} P_{\mathrm{T}_{\mathrm{S}}}}{P_{\mathrm{T}_{\mathrm{S}}} P_{\mathrm{T}_{\mathrm{I}}}}\right) \mathrm{d}r_{\mathrm{I}}. \tag{21}$$

By substituting the value of $\sigma_{\tilde{\dot{V}}_{\mathrm{S}}}$ given in (15) into (21), we get the solution as given in (22).

Case II: This special case represents the scenario when the rate of fluctuation in the interference channel is much higher than that in the desired channel, i.e., $N_{R_{\mathrm{I}}} \gg N_{R_{\mathrm{S}}}$. The SIR level of observation can be defined as $\widetilde{R}_\eta = \frac{r_{\mathrm{S}}^2}{\widetilde{R}_{\mathrm{I}}^2 P_{\mathrm{T}_{\mathrm{I}}}}$, and the LCR expression of the SIR can be derived as follows,

$$N_{R_\eta} \cong \int_0^\infty \frac{\left(\frac{r_{\mathrm{S}}^2}{P_{\mathrm{T}_{\mathrm{I}}}\widetilde{R}_\eta}\right)^{m_{\mathrm{I}}-\frac{1}{2}} m_{\mathrm{S}}^{m_{\mathrm{S}}} m_{\mathrm{I}}^{m_{\mathrm{I}}-\frac{1}{2}} r_{\mathrm{S}}^{2m_{\mathrm{S}}-1}}{\Gamma(m_{\mathrm{I}})\Gamma(m_{\mathrm{S}})\sqrt{3}P_{\mathrm{T}_{\mathrm{S}}}^{m_{\mathrm{S}}}} \times \sigma_{\tilde{\dot{V}}_{\mathrm{I}}} \omega_{\max} \sqrt{P_{\mathrm{T}I}} \exp\left(\frac{-r_{\mathrm{S}}^2 P_{\mathrm{T}_{\mathrm{I}}} m_{\mathrm{S}} \widetilde{R}_\eta + m_{\mathrm{I}} P_{\mathrm{T}_{\mathrm{S}}}}{P_{\mathrm{T}_{\mathrm{S}}} P_{\mathrm{T}_{\mathrm{I}}} \widetilde{R}_\eta}\right) \mathrm{d}r_{\mathrm{S}}. \tag{23}$$

By substituting the equation for $\sigma_{\tilde{\dot{V}}_{\mathrm{I}}}$ given by (15) in (23), and performing simplifications operations, the solution can be expressed as given in (24).

D. AVERAGE FADE DURATION (AFD)

AFD can be found from LCR and PDF of fading envelope as,

$$\bar{\tau}_R = \frac{1}{N_R} \int_0^R f_r(r) \mathrm{d}r. \tag{25}$$

After substituting the expression of LCR given in (19) and the PDF of signal envelope given in (17) into (25), a simplified expression for AFD can be obtained as,

$$\bar{\tau}_{R_{(\cdot)}} = \frac{\sqrt{\pi P_{\mathrm{T}_{(\cdot)}}} \left[\Gamma(m_{(\cdot)}) - \hat{\Gamma}\left(m_{(\cdot)}, \frac{m_{(\cdot)}\widetilde{R}_{(\cdot)}^2}{P_{\mathrm{T}_{(\cdot)}}}\right)\right]}{\sigma_{\tilde{\dot{V}}_{(\cdot)}} \widetilde{R}_{(\cdot)}^{(2m_{(\cdot)}-1)} m_{(\cdot)}^{(m_{(\cdot)}-1/2)} \exp\left(-m_{(\cdot)}\widetilde{R}_{(\cdot)}^2\right)}, \tag{26}$$

where the $\hat{\Gamma}(.,.)$ is the incomplete Gamma function. By substituting the individual arrangement of the multipath shape factor for interference $\bar{\tau}_{R_{\mathrm{I}}}$ and desired signal $\bar{\tau}_{R_{\mathrm{S}}}$ in (26), independent analysis can be conducted. In V2V propagation

environments, due to rapid time variations observed in the channel statistics, large-scale variations in the fade's duration are observed which further limit the efficient utilization of different channel coding schemes. This can potentially result in causing non-stationary burst error condition [54]. Therefore, it is important to thoroughly investigate the behaviour of fades duration for such V2V scenarios. AFD for jointly studying the interference and desired channels (i.e., in terms of SIR) can be defined as,

$$\bar{\tau}_{R_\eta} = \frac{I_{\ddot{\Omega}}(m_{\mathrm{S}}, m_{\mathrm{I}})}{N_{R_\eta}}, \tag{27}$$

where

$$\ddot{\Omega} = \frac{m_{\mathrm{S}}\widetilde{R}_\eta}{m_{\mathrm{S}}\widetilde{R}_\eta + m_{\mathrm{I}}}, \tag{28}$$

and $I_{(\cdot)}(.,.)$ represents the Incomplete Beta function. Simplified solution for $\bar{\tau}_{R_\eta}$ can be obtained by substituting the expression of N_{R_η} from (20) into (27) and performing mathematical simplifications. The two special cases discussed for LCR can also be extended to derive expressions AFD for the cases. By substituting (22) and (24), as shown at the bottom of the this page, into (27), the AFD expressions for the two specials cases can be obtained.

E. SPATIAL AUTO-COVARIANCE (SAC)

Another important second-order fading statistic quantifier of the received signal envelope is SAC. The SAC for independent interference and desired channels in V2V context (where the separation distance between commnunicating nodes is taken as l) can be derived, by extending the expression given in [6] for F2V mobility context, given as follows,

$$\varrho_{(\cdot)}(l) = \frac{\mathbb{E}\left[r_{(\cdot)}\{\vec{\mathbf{l}}_0\} r_{(\cdot)}\{\vec{\mathbf{l}}_0 + l\hat{\mathbf{l}}\}\right] - \mathbb{E}^2\left[r_{(\cdot)}\right]}{\mathbb{E}\left[r^2_{(\cdot)}\right] - \mathbb{E}^2\left[r_{(\cdot)}\right]}, \tag{29}$$

where the parameters $\vec{\mathbf{l}}_0$ and $\hat{\mathbf{l}}$ represent the relative reference spatial position of the nodes and the unit vector representing the direction pointing along the relative direction of nodes mobility in 3-D space, respectively. The separation distance l is a function of direction of motion of the communicating nodes (i.e., α_p, β_p, α_q, and β_q) and their velocities (v_p and v_q). After reinterpreting the definition of SAC presented in [6] from F2V to V2V mobility context, the approximate envelope correlation function for independent characterization of desired and interference channels can be expressed in simplified form as,

$$\varrho_{(\cdot)}(l) \approx \exp\left\{\left(\frac{l}{\lambda}\right)^2 \frac{\sigma^2_{\dot{\tilde{V}}_{(\cdot)}}}{\omega^2_{\max} P_{\mathrm{T}_{(\cdot)}}} \times \frac{-m_{(\cdot)}\Gamma^2(m_{(\cdot)})}{\left(m_{(\cdot)}\Gamma^2(m_{(\cdot)}) - \Gamma^2(m_{(\cdot)} + \frac{1}{2})\right)}\right\}. \tag{30}$$

From (30), the envelope correlation for the interference and desired signal (i.e., $\varrho_{\mathrm{I}}(l)$ and $\varrho_{\mathrm{S}}(l)$) can be determined

$$N_{R_\eta} \cong \int_0^\infty \frac{\left(\frac{\widetilde{R}_\eta r_{\mathrm{I}}^2}{P_{\mathrm{T_S}}}\right)^{m_{\mathrm{S}}-\frac{1}{2}} m_{\mathrm{I}}^{m_{\mathrm{I}}} m_{\mathrm{S}}^{m_{\mathrm{S}}-\frac{1}{2}} r_{\mathrm{I}}^{2m_{\mathrm{I}}-1}}{\Gamma(m_{\mathrm{S}})\Gamma(m_{\mathrm{I}})\sqrt{3}P_{\mathrm{T_I}}^{m_{\mathrm{I}}}} \times \left\{\Upsilon^2_{p_{\mathrm{S}}}\left(1 + \frac{3}{2}\left(\xi_{p_{\mathrm{S}}}\left(2\sin^2\varphi_{v_p} - \frac{2}{3}\right) + \chi_{p_{\mathrm{S}}}\sin\left(2\varphi_{v_p}\right)\right.\right.\right.$$
$$\times \cos\left(\vartheta_{v_p} - \phi^{\max}_{\beta_p 45_{\mathrm{S}}}\right) + \zeta_{p_{\mathrm{S}}}\cos^2\varphi_{v_p}\cos\left(2\left(\vartheta_{v_p} - \phi^{\max}_{\beta_p 0_{\mathrm{S}}}\right)\right)\Big)\Big) + \Upsilon^2_{q_{\mathrm{S}}}\Big(1 + \frac{3}{2}\Big(\xi_{q_{\mathrm{S}}} \times \Big(2\sin^2\varphi_{v_q} - \frac{2}{3}\Big)$$
$$+\chi_{q_{\mathrm{S}}}\sin 2\varphi_{v_q}\cos\left(\vartheta_{v_q} - \phi^{\max}_{\beta_q 45_{\mathrm{S}}}\right) + \zeta_{q_{\mathrm{S}}}\cos^2\varphi_{v_q}\cos\left(2\left(\vartheta_{v_q} - \phi^{\max}_{\beta_q 0_{\mathrm{S}}}\right)\right)\Big)\Big) + \left(\Upsilon^2_{p_{\mathrm{S}}} + \Upsilon^2_{q_{\mathrm{S}}}\right)\Big(\Xi_{\mathrm{S}}\sin\varphi_{v_p}\sin\varphi_{v_q}$$
$$+\Delta_{+_{\mathrm{S}}}\cos\left(\vartheta_{v_p} - \vartheta_{v_q} - \left(\phi^{\max}_{pq0_{\mathrm{S}}} - \phi^{\max}_{qp0_{\mathrm{S}}}\right)\right) + \Delta_{-_{\mathrm{S}}}\cos\left(\vartheta_{v_p} + \vartheta_{v_q} - \left(\phi^{\max}_{pq0_{\mathrm{S}}} + \phi^{\max}_{qp0_{\mathrm{S}}}\right)\right) + \kappa^q_{p_{\mathrm{S}}}\cos\left(\vartheta_{v_p} - \phi^{\max}_{p/\beta_q{}_{\mathrm{S}}}\right)$$
$$\times \sin\varphi_{v_q} + \kappa^p_{q_{\mathrm{S}}}\cos\left(\vartheta_{v_q} - \phi^{\max}_{q/\beta_p{}_{\mathrm{S}}}\right)\sin\varphi_{v_p}\Big)\Big\}^{\frac{1}{2}} \omega_{\max}\sqrt{P_{\mathrm{TS}}}\exp\left(\frac{-r_{\mathrm{I}}^2 P_{\mathrm{T_I}} m_{\mathrm{S}}\widetilde{R}_\eta + m_{\mathrm{I}}P_{\mathrm{TS}}}{P_{\mathrm{T_S}}P_{\mathrm{T_I}}}\right)\mathrm{d}r_{\mathrm{I}}. \tag{22}$$

$$N_{R_\eta} \cong \int_0^\infty \frac{\left(\frac{r_{\mathrm{S}}^2}{P_{\mathrm{T_I}}\widetilde{R}_\eta}\right)^{m_{\mathrm{I}}-\frac{1}{2}} m_{\mathrm{S}}^{m_{\mathrm{S}}} m_{\mathrm{I}}^{m_{\mathrm{I}}-\frac{1}{2}} r_{\mathrm{S}}^{2m_{\mathrm{S}}-1}}{\Gamma(m_{\mathrm{I}})\Gamma(m_{\mathrm{S}})\sqrt{3}P_{\mathrm{T_S}}^{m_{\mathrm{S}}}} \Big\{\Upsilon^2_{p_{\mathrm{I}}}\Big(1 + \frac{3}{2}\Big(\xi_{p_{\mathrm{I}}}\Big(2\sin^2\varphi_{v_p} - \frac{2}{3}\Big) + \chi_{p_{\mathrm{I}}}\sin\left(2\varphi_{v_p}\right)$$
$$\times \cos\left(\vartheta_{v_p} - \phi^{\max}_{\beta_p 45_{\mathrm{I}}}\right) + \zeta_{p_{\mathrm{I}}}\cos^2\varphi_{v_p} \times \cos\left(2\left(\vartheta_{v_p} - \phi^{\max}_{\beta_p 0_{\mathrm{I}}}\right)\right)\Big)\Big) + \Upsilon^2_{q_{\mathrm{I}}}\Big(1 + \frac{3}{2}\Big(\xi_{q_{\mathrm{I}}}\Big(2\sin^2\varphi_{v_q} - \frac{2}{3}\Big)$$
$$+\chi_{q_{\mathrm{I}}}\sin 2\varphi_{v_q}\cos\left(\vartheta_{v_q} - \phi^{\max}_{\beta_q 45_{\mathrm{I}}}\right) + \zeta_{q_{\mathrm{I}}}\cos^2\varphi_{v_q}\cos\left(2\left(\vartheta_{v_q} - \phi^{\max}_{\beta_q 0_{\mathrm{I}}}\right)\right)\Big)\Big) + \left(\Upsilon^2_{p_{\mathrm{I}}} + \Upsilon^2_{q_{\mathrm{I}}}\right)\Big(\Xi_{\mathrm{I}}\sin\varphi_{v_p}\sin\varphi_{v_q}$$
$$+\Delta_{+_{\mathrm{I}}}\cos\left(\vartheta_{v_p} - \vartheta_{v_q} - \left(\phi^{\max}_{pq0_{\mathrm{I}}} - \phi^{\max}_{qp0_{\mathrm{I}}}\right)\right) + \Delta_{-_{\mathrm{I}}}\cos\left(\vartheta_{v_p} + \vartheta_{v_q} - \left(\phi^{\max}_{pq0_{\mathrm{I}}} + \phi^{\max}_{qp0_{\mathrm{I}}}\right)\right) + \kappa^q_{p_{\mathrm{I}}}\cos\left(\vartheta_{v_p} - \phi^{\max}_{p/\beta_q{}_{\mathrm{I}}}\right)$$
$$\times \sin\varphi_{v_q} + \kappa^p_{q_{\mathrm{I}}}\cos\left(\vartheta_{v_q} - \phi^{\max}_{q/\beta_p{}_{\mathrm{I}}}\right)\sin\varphi_{v_p}\Big)\Big\}^{\frac{1}{2}} \omega_{\max}\sqrt{P_{\mathrm{TI}}}\exp\left(\frac{-r_{\mathrm{S}}^2 P_{\mathrm{T_I}} m_{\mathrm{S}}\widetilde{R}_\eta + m_{\mathrm{I}}P_{\mathrm{TS}}}{P_{\mathrm{T_S}}P_{\mathrm{T_I}}\widetilde{R}_\eta}\right)\mathrm{d}r_{\mathrm{S}}. \tag{24}$$

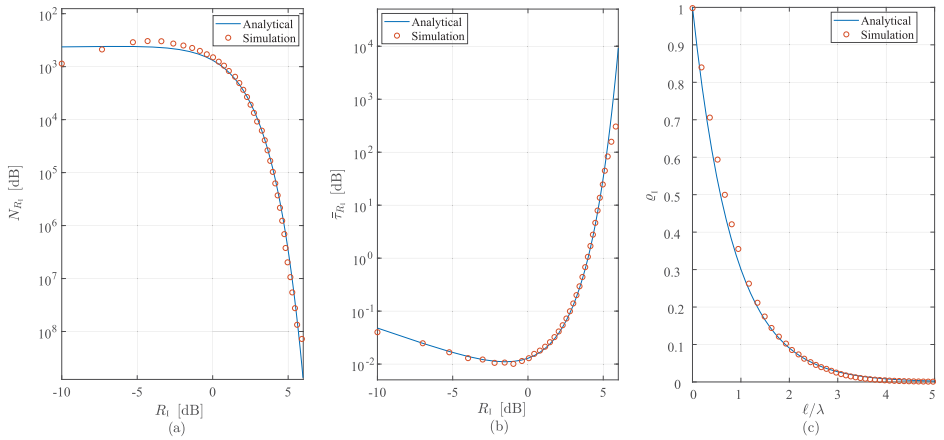

FIGURE 4. Comparison of simulation and analytical results for (a) LCR, (b) AFD, and (c) SAC.

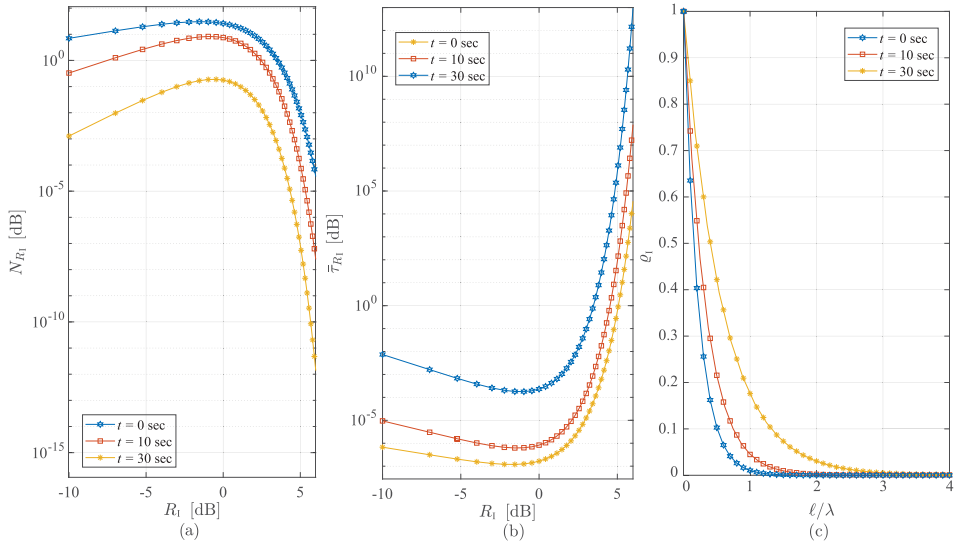

FIGURE 5. Demonstration of modeling time-variation through the derived expressions of (a) LCR, (b) AFD, and (c) SAC. The second-order fading statistics plotted at different time-snaps correspond to different stationary increments of the non-stationary channel.

by appropriately utilizing the corresponding set of multi-path shape factors for the both channels. CD is the distance between two points at which the spatial correlation remains higher than 0.5 (i.e., $\varrho_{(\cdot)}(l = D_c) \geq 0.5$). The expression derived for CD in [6] for F2V communication context can be extended to V2V communications context. The simplified solution can be expressed as,

$$D_{c_{(\cdot)}} = \frac{\lambda\, \omega_{\max}}{\sigma_{\dot{\tilde{V}}_{(\cdot)}}} \left\{ \sqrt{\ln(2) P_{\mathrm{T}_{(\cdot)}}} \times \sqrt{\frac{\left(m_{(\cdot)} \Gamma^2(m_{(\cdot)}) - \Gamma^2(m_{(\cdot)} + \frac{1}{2}) \right)}{m_{(\cdot)} \Gamma^2(m_{(\cdot)})}} \right\}. \quad (31)$$

The CD is of high importance in measuring the spatial selective behaviour of the channels. This analysis can further be extended to jointly studying the SAC for interference and desired channels (i.e., against SIR). To this end, the definition of SAC against SIR, $\varrho_\eta(l)$, as proposed in [6] can be given by,

$$\varrho_\eta(l) = \frac{\mathbb{E}\left[\Theta_\eta(l)\right] - \mathbb{E}^2[\eta]}{\mathbb{E}\left[\eta^2\right] - \mathbb{E}^2[\eta]}, \quad (32)$$

where $\Theta_\eta(l) = \eta\{\vec{\mathbf{l}}_0\}\eta\{\vec{\mathbf{l}}_0 + l\hat{\mathbf{l}}\}$ and its statistical expectation can be expressed as given in [6], as follows,

$$\mathbb{E}\left[\Theta_\eta(l)\right] = \frac{\mathbb{E}^2[\Theta_{\mathrm{S}}(l)]}{\mathbb{E}^2[\Theta_{\mathrm{I}}(l)]} + \frac{3\, P_{T_{\mathrm{I}}}^2 \mathbb{E}^2[\Theta_{\mathrm{S}}(l)]}{m_{\mathrm{I}} \mathbb{E}^4[\Theta_{\mathrm{I}}(l)]} + \frac{P_{T_{\mathrm{S}}}^2}{m_{\mathrm{S}} \mathbb{E}^2[\Theta_{\mathrm{I}}(l)]}, \quad (33)$$

where $\mathbb{E}[\Theta_{(\cdot)}(l)]$ for both interference and desired channels can be obtained as,

$$\mathbb{E}\left[\Theta_{(\cdot)}(l)\right] = \varrho_{(\cdot)}(l) \left(P_{T_{(\cdot)}} - \frac{P_{T_{(\cdot)}}}{m_{(\cdot)}} \left(\frac{\Gamma(m_{(\cdot)} + 1/2)}{\Gamma(m_{(\cdot)})} \right)^2 \right) + \frac{P_{T_{(\cdot)}}}{m_{(\cdot)}} \left(\frac{\Gamma\left(m_{(\cdot)} + 1/2\right)}{\Gamma(m_{(\cdot)})} \right)^2. \quad (34)$$

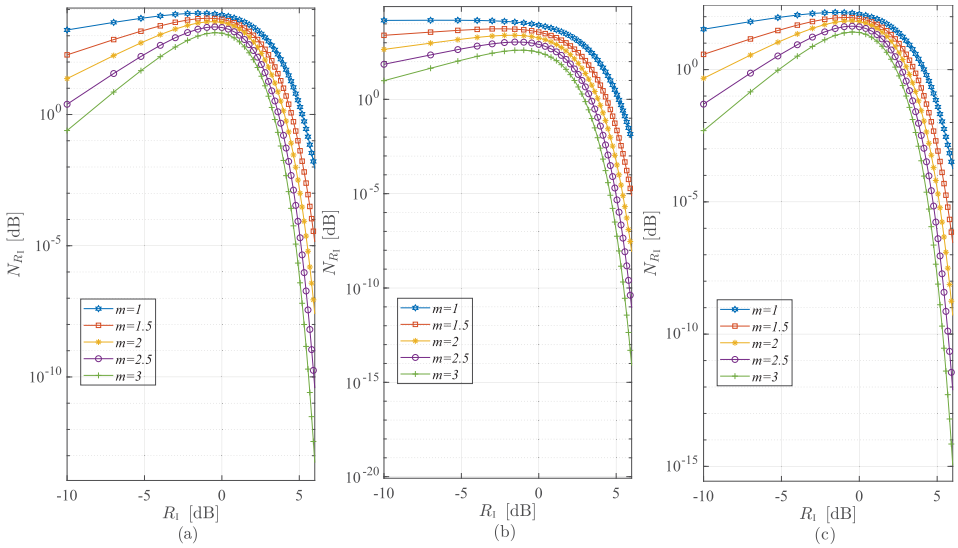

FIGURE 6. The effect of change in the threshold level and the Nakagami *m* parameter on LCR (for a typical stationary region of small-scale channel fading) for different inter-vehicular communication contexts; (a) AV2AV mobility context for $|\vartheta_{v_p} - \vartheta_{v_q}| = 180°$, $|\varphi_{v_p} - \varphi_{v_q}| = 10°$, (b) AV2GV mobility context for $|\vartheta_{v_p} - \vartheta_{v_q}| = 0°$, $|\varphi_{v_p} - \varphi_{v_q}| = 35°$, and (c) GV2GV mobility context for $|\vartheta_{v_p} - \vartheta_{v_q}| = 180°$, $|\varphi_{v_p} - \varphi_{v_q}| = 0°$.

The solution for $\mathbb{E}\left[\eta^2\right]$ provided in [6] can be reinterpreted for the proposed context of V2V communications. By substituting the above findings in (32), the SAC can be studied against SIR in V2V communication context.

2-D spatial channel models provide computational simplicity; however this simplicity has an associated cost of compromised accuracy in the description of propagation behaviour. Notably, in AV2GV propagation environments, it is highly essential not to ignore the elevation axis while modeling the scattering behaviour. Furthermore, for the vehicular propagation channels, where the scattering environment in the vicinity of both the link ends is vastly different from each other, the simplification technique of transforming dual-end mobility into a single-end relative mobility context (i.e., assuming one link-end as static and other as relatively mobile) does not hold. The proposed expressions take a more accurate 3-D description of scattering environments into account, model the scattering environment in the vicinity of both the link-ends, and jointly investigate both desired and interference channels (i.e., against SIR); therefore, there is an additional cost of complexity also associated to the derived expressions.

IV. RESULTS AND EVALUATIONS

This section conducts a performance evaluation of the proposed framework for the characterization of interference of inter-vehicular communication networks in the 3-D angular domain. The 3-D communication context illustrated in Fig. 2 is considered for the analysis conducted in this section (i.e., composed of AV2GV and GV2GV links). Any channel model which provides spatial description of the considered radio propagation environment can be utilized with the expressions derived in this paper for jointly studying the second-order fading statistics of interference and desired channels. In this context, a simple 3D ellipsoidal channel model described in Sec. II is utilized to conduct the analysis and demonstrate the usefulness of the derived expressions for channel fading statistics. This fact underlies all the results and discussion provided in this section. However, it is pertinent to highlight that the use of the derived expressions are not restricted to the considered 3D ellipsoidal channel model.

To analyze the fading statistics of a specific scenario, the jPDF of 3-D AoA and 3-D AoD for the considered propagation scene can be taken from a suitable analytical channel model, or it can be generated through computer simulations in a single or multi-cluster propagation modeling context. In the conducted analysis, the jPDF is generated through computer simulations for both single- and multi-cluster scattering environments. In a multi-cluster scattering scenario, the amount of scattering clusters is drawn from Poisson distribution with its intensity proportional to the volume of considered geographic region, while the spatial position (coordinates of origin) of the clusters is drawn from uniform distribution confined within the defined 3-D spatial geographic region. The scattering clusters (interference and desired) are modeled as spherical shaped with their radius drawn from uniform distribution between the range 40m to 80m. The number of SP in each cluster are drawn from Poisson distribution with its intensity proportional to the volume of the cluster, and the SP within each group are taken as uniformly distributed. The spatial position of the desired and interfering nodes is drawn from uniform distribution within a defined suitable range based on the under consideration communication context of AV2GV or GV2GV, e.g., the altitude for the AV nodes is drawn between the range 50m to 150m. For the results obtained for a single scattering cluster scenario, the interfering cluster is fixed as of 100m radius, and

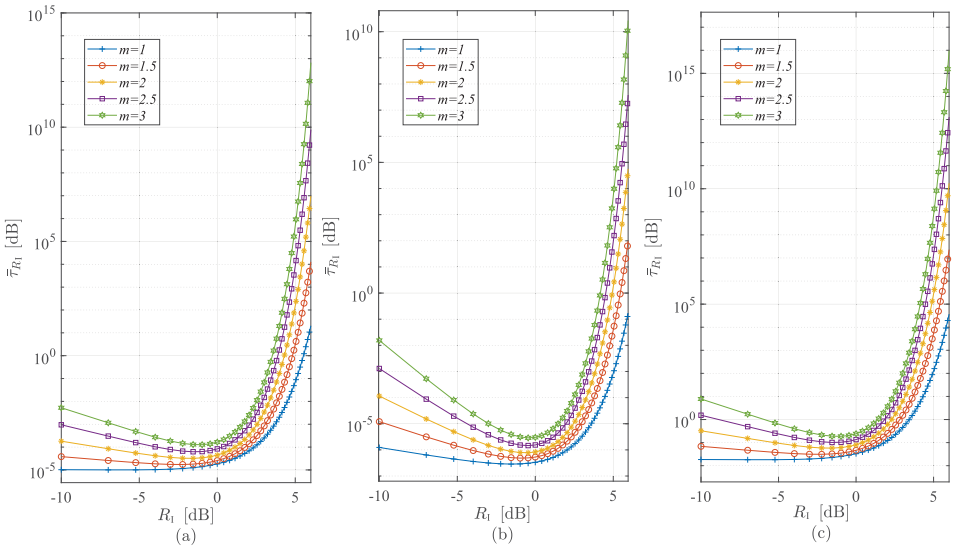

FIGURE 7. The effect of change in the threshold level and the Nakagami *m* parameter on AFD (for a typical stationary region of small-scale channel fading) for different inter-vehicular communication contexts; (a) AV2AV mobility context for $|\vartheta_{v_p} - \vartheta_{v_q}| = 180°$, $|\varphi_{v_p} - \varphi_{v_q}| = 10°$, (b) AV2GV mobility context for $|\vartheta_{v_p} - \vartheta_{v_q}| = 0°$, $|\varphi_{v_p} - \varphi_{v_q}| = 35°$, and (c) GV2GV mobility context for $|\vartheta_{v_p} - \vartheta_{v_q}| = 180°$, $|\varphi_{v_p} - \varphi_{v_q}| = 0°$.

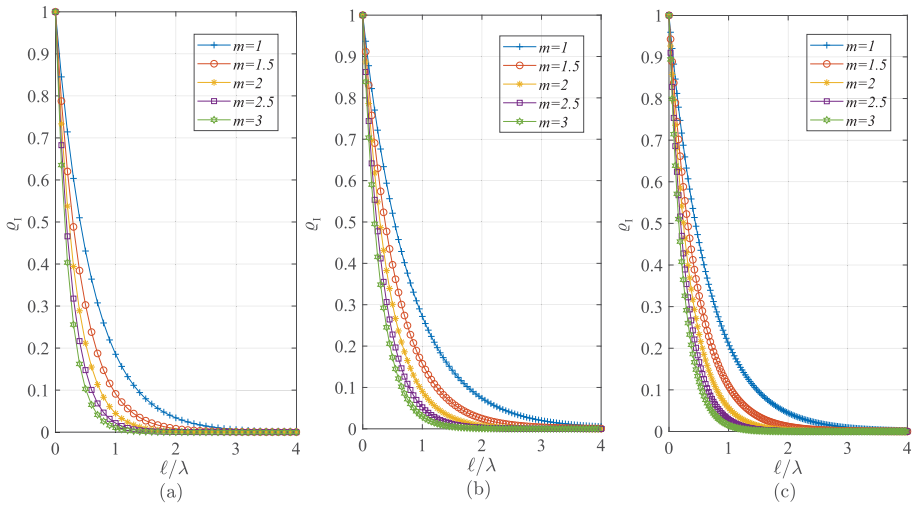

FIGURE 8. The effect of change in the spatial separation between nodes normalized by the wavelength and the Nakagami *m* parameter on SAC (for a typical stationary region of small-scale channel fading) for different inter-vehicular communication contexts; (a) AV2AV mobility context for $|\vartheta_{v_p} - \vartheta_{v_q}| = 180°$, $|\varphi_{v_p} - \varphi_{v_q}| = 10°$, (b) AV2GV mobility context for $|\vartheta_{v_p} - \vartheta_{v_q}| = 0°$, $|\varphi_{v_p} - \varphi_{v_q}| = 35°$, and (c) GV2GV mobility context for $|\vartheta_{v_p} - \vartheta_{v_q}| = 180°$, $|\varphi_{v_p} - \varphi_{v_q}| = 0°$.

the cluster contains 500 SP taken as uniformly distributed. For example, the spatial position (origin of the cluster) of the cluster (interference or desired) is taken at coordinates (500, 500, $z_{C_{(\cdot),g}}$). Different values for $z_{C_{(\cdot),g}}$ are studied to investigate the importance of elevation of the scattering clusters on the fading statistics.

For independent characterization of fading statistics of interference channels in GV2GV communication scenario, the direction of motion of the communicating nodes (e.g., p^{th} and q^{th} node) in azimuth and elevation planes are set to be $\{\vartheta_{v_p} = 180°, \vartheta_{v_q} = 0°\}$ and $\{\varphi_{v_p} = 0°, \varphi_{v_q} = 0°\}$, respectively. Similarly, for the taken AV2GV communication scenario, the direction of motion of the nodes in azimuth and elevation planes are set to be $\{\vartheta_{v_p} = 90°, \vartheta_{v_q} = 90°\}$ and $\{\varphi_{v_p} = 0°, \varphi_{v_q} = 35°\}$, respectively. The receiving node, desired transmitting node, and interference transmitting node are taken as mobile with the velocity of 10m/s, 5m/s, and 5m/s, respectively, and carrier frequency f_c is taken as 2000MHz. Moreover, the fading severity parameter is also varied over a reasonable range (to cover Rayleigh, Rician, and other fading conditions). For AV2AV communication environment, the value for $z_{C_{(\cdot),g}}$ is drawn from uniform distribution in the range from 40m to 100m. The simulation and analytical results for second-order fading statistics of

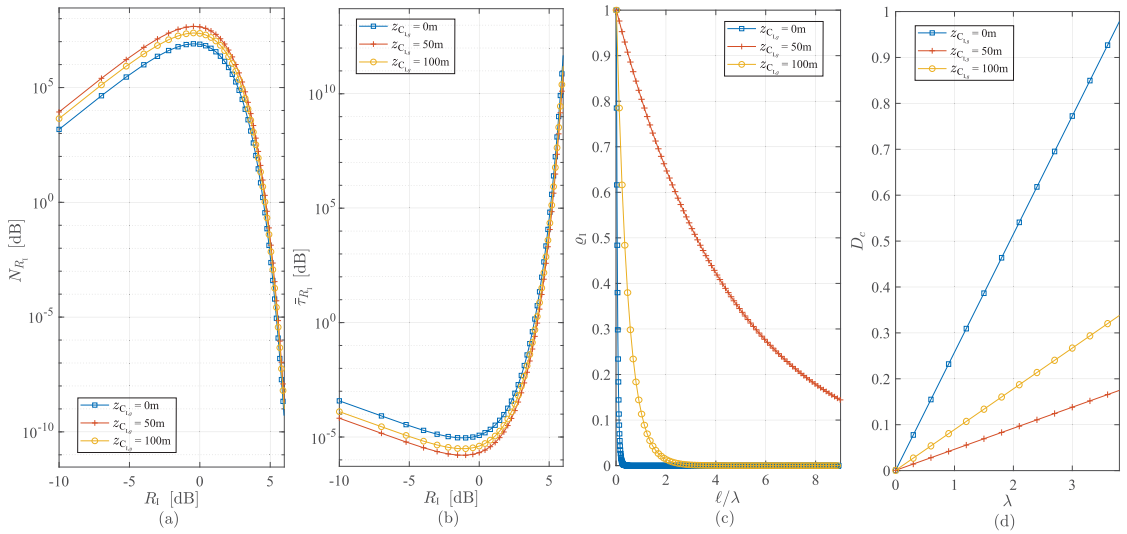

FIGURE 9. For a single-cluster scenario, the impact of spatial position of interfering cluster on LCR, AFD, SAC, and CD (for a typical stationary region of small-scale channel fading) of interference signal in (a),(b),(c), and (d), respectively.

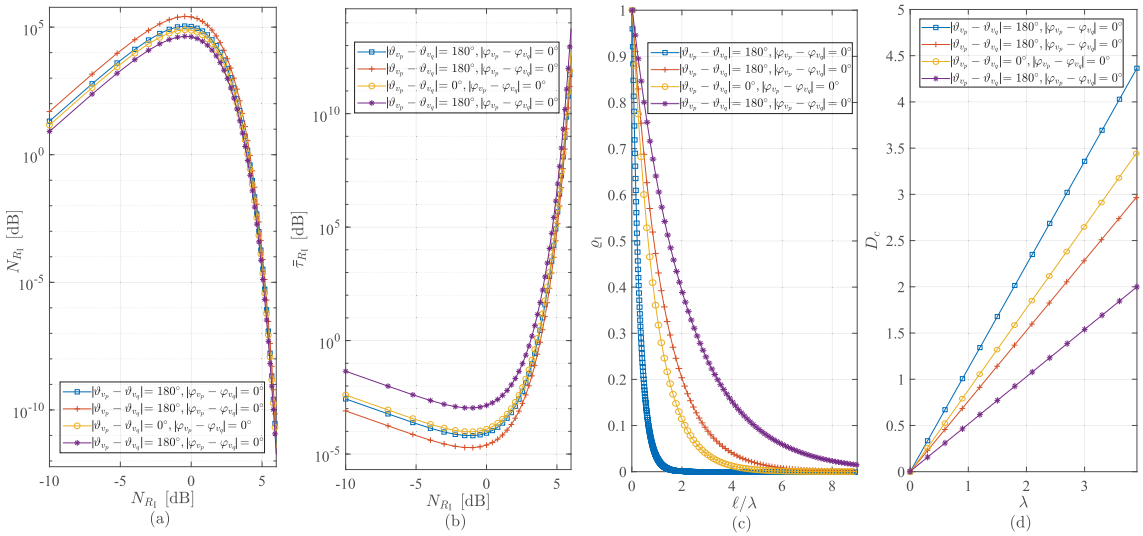

FIGURE 10. The impact of direction of mobility of communicating nodes on LCR, AFD, SAC, and CD (for a typical stationary region of small-scale channel fading) of interference channel for a single-cluster scattering scenario in (a),(b),(c), and (d), respectively.

interference signals obtained for a single cluster scenario are compared in Fig. IV. All the physical model parameters are set as exactly the same values for obtaining both simulation and analytical results. The coordinates of scattering points within the scattering cluster are drawn from homogeneous Poisson point process (HPPP) with an intensity $\lambda_{\mathrm{SP}} = 0.02$. The computer simulations are performed by following the approach presented in Chap. 5 of [55] for simulation of wireless propagation channels for characterizing second-order fading statistics. The simulation results are averaged over 10^4 Monte carlo runs. Mean-square-error (MSE) can be used as a goodness-of-fit metric. The MSE between the analytical and simulation plots in Fig. (a), (b), and (c) is observed to be 0.0371, 0.0518, and 0.0867, respectively, which can be regarded as a good match.

The time-snaps of LCR and AFD against threshold level, and SAC against the spatial separation between nodes normalized by the wavelength of interference channel representing the results for three widely separated time-windows of received signal envelopes in Fig. 5 (a), (b), and (c), respectively. The mobility of nodes is set such that the LoS link distance is decreasing with increasing time. These time snapshots represent the second-order fading statistics of the received signal envelope at widely separated spatial positions of the nodes along their mobility route, where the channel statistics become non-stationary (i.e., correlation is $\leq 50\%$). In Fig. 6, the impact of variation in Nakagami shape factor m on LCR against the threshold level is investigated. In Fig. 6(a), (b), and (c), the AV2AV, AV2GV and GV2GV communicating environments are focused on the considered direction of motions in 3-D space, respectively. It is observed that regardless of the direction of motion of communicating nodes, the average trend of LCR is decreasing over the threshold level. However, the whole curve of LCR is shifted

downward with the increase in Nakagami shape factor m. The same considered assumptions are used to find the effect of increasing Nakagami shape factor m on AFD against the threshold and SAC against the ratio of separation distance to the wavelength, moreover, the results are plotted in Fig. 7 and Fig. 8, respectively. Independent of the direction of motion of communicating nodes the overall behavior of AFD is increasing over different values of the threshold. However, the whole curve of AFD is shifted upward with the increase in Nakagami shape factor m. Furthermore, the overall trend of SAC gives vertical dilation when we increase the value of Nakagami shape factor m.

The spatial position of the interfering cluster depends upon the composition of radio propagation environment. For the considered scenario, different spatial positions for the origin of the interfering cluster is taken, i.e., elevated from the ground as $z_{C_{\mathrm{I},g}} = 50$ and $z_{C_{\mathrm{I},g}} = 100$. The directions of motion in azimuth and elevation planes for AV2GV scenario in such conditions are taken as, $\{\vartheta_{v_p} = 90^\circ, \vartheta_{v_q} = 90^\circ\}$ and $\{\varphi_{v_p} = 0^\circ, \varphi_{v_q} = 35^\circ\}$, respectively. So, the effect of change in the spatial position of interfering cluster on LCR, AFD, SAC and CD is shown in Fig. 9 (a), (b), (c), and (d), respectively, furthermore, Nakagami shape factor m is set to be 3.

For the considered AV2AV communicating environment, the four particular types of directional motions for example, away from each other (i.e. $\{\vartheta_{v_p} = 0^\circ$ and $\vartheta_{v_p} = 180^\circ\}$), towards each other (i.e. $\{\vartheta_{v_p} = 180^\circ$ and $\vartheta_{v_p} = 0^\circ\}$), parallel to each other (i.e. $\{\vartheta_{v_p} = 90^\circ$ and $\vartheta_{v_p} = 90^\circ\}$) and non-parallel to each other (i.e. $\{\vartheta_{v_p} = 90^\circ$ and $\vartheta_{v_p} = 270^\circ\}$) are analyzed in Fig. 10. In Fig. 10(a), (b), (c) and (d) the joint comparison for such directional motions are depicted for LCR, AFD, SAC and CD, respectively.

The impact of variations in SIR, interference channel's fading shape factor m_{I}, and desired channel's fading shape factor m_{S} on LCR is shown in Fig. 11. The set of sub-figures {(a), (b)} and {(c), (d)} represent the results for the discussed two special cases $\{N_{R_{\mathrm{I}}} \ll N_{R_{\mathrm{S}}}\}$ and $\{N_{R_{\mathrm{I}}} \gg N_{R_{\mathrm{S}}}\}$. In Fig. 11 (a) and (c) the value of the desired signal's Nakagami fading shape factor m_{S} is set as 3 while the interference channel's fading shape factor m_{I} is varied in the range between 1 and 5. In Fig. 11 (b) and (d), the value of interference channel's fading shape factor m_{I} is set as 3, while the impact of changes in desired signal's fading shape factor m_{S} is demonstrated. For the first special case, when observing along the axis representing SIR threshold R_η, a non-linear decrease in N_{R_η} can be observed. However, for the second special case, a converse behaviour can be seen.

By adopting the same approach as applied for the analysis conducted for LCR of SIR (i.e., N_{R_η}), for the two special cases, the AFD $\bar{\tau}_{R_\eta}$ can also be analysed, as plotted in Fig. 12. To analyse the AFD of SIR ($\bar{\tau}_{R_\eta}$) the first special case is plotted in the set of figures {Fig. 12 (a) and (b)}, while the set of figures {Fig. 12 (c) and (d)} represents the second special case.

TABLE 4. Substitutions required in proposed model parameters to deduce other notable spatial interference models.

Model	Substitutions Required
Chen et al. [38], 2014	$\vartheta_{v_p} = 0^\circ$, $\varphi_{v_p} = 0^\circ$, $\beta_p \to 0^\circ$, $\beta_q \to 0^\circ$, and $v_p = 0$m/s
Nawaz et al. [6], 2017	$\vartheta_{v_p} = 0^\circ$, $\varphi_{v_p} = 0^\circ$, and $v_p = 0$m/s
Du et al. [36], 2019	$\vartheta_{v_p} = 0^\circ$, $\varphi_{v_p} = 0^\circ$, and $v_p = 0$m/s

The proposed framework for the characterization of second-order fading statistics of desired and interference channels is a generalized framework which can be deduced to a few notable existing models available in the literature. The considered realistic amount of spatial dimensions for the radio waves propagation, mobility as possible for all the nodes, and flexibility in the direction of mobility of the nodes has enabled in achieving this generalization of the proposed framework. The list of substitutions required to deduce the proposed framework to the existing works is given in Table 4. This generalization property of the derived equations also establishes their validity. The conducted study is of high significance in designing of the multi-antenna inter-vehicular communication transceivers. The angular characteristics of the radio channels are of high importance in designing of the antenna-elements separation in order to optimally steer the beams and nulls towards the desired and interfering nodes, respectively. Furthermore, this study can also be used as a reference point for designing and studying of error correction coding schemes (e.g., interleaving etc) in various interesting inter-vehicular future HetNets, such as UAVs-assisted cell-free communications. Moreover, the accurate understanding of physical directions that substantially contribute in the increase in fading rate (i.e., shape factor indicating direction of maximum fading) for both interference and desired channels in a certain inter-vehicular radio propagation scenario can also help in optimally integrating the intelligent reflective surfaces within the considered environment for creating favourable propagation conditions.

The conducted analysis is of high significance in designing and performance evaluation of high-capacity transmission schemes in interference-limited wireless networks, as well as in various aspects of transceiver designing, error-correcting codes designing, and channel parameter estimation, etc. The potential research directions for the extension of this work are indicated as follows. Conducting a comprehensive study to establish a direct analytical relationship between the shape parameter m of Nakagami-m fading channels with the spatial parameters representing the composition of scattering environment is of high importance. Moreover, investigation of second-order fading statistics against SIR by considering more generalized distribution for representing the fading behaviour of desired and interference channels, such as κ-μ distribution, η-μ distribution, α-η-μ distribution, and α-κ-μ distribution, is another potential direction for extension of this research work. The relationship of wireless channel fading statistics with wireless network topology is another important

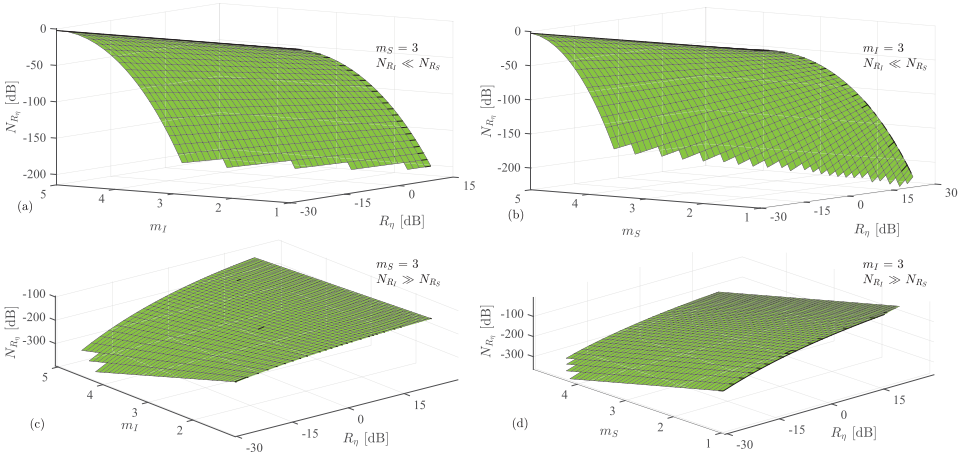

FIGURE 11. The impact of SIR and fading shape factor of interference (m_I) and desired (m_S) channels on joint LCR (for a typical stationary region of small-scale channel fading). The set of sub-figures {(a), (b)} and {(c), (d)} represent the two special cases $\{N_{R_I} \ll N_{R_S}\}$ and $\{N_{R_I} \gg N_{R_S}\}$, respectively.

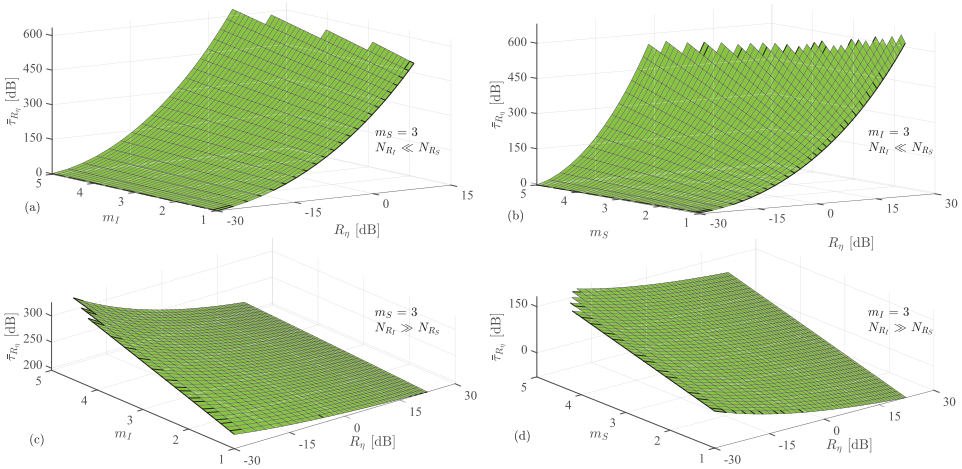

FIGURE 12. The impact of SIR and fading shape factor of interference (m_I) and desired (m_S) channels on joint AFD (for a typical stationary region of small-scale channel fading). The set of sub-figures {(a), (b)} and {(c), (d)} represent the two special cases $\{N_{R_I} \ll N_{R_S}\}$ and $\{N_{R_I} \gg N_{R_S}\}$, respectively.

direction for extending this work. Furthermore, The proposed analytical framework is of high significance to be used as a reference for conducting the measurement campaigns in the future, in order to intensively study and model the second-order statistics of network interference.

V. CONCLUSION

Spatial modeling of interference in a 3-D volumetric inter-vehicular communication context (e.g., AV2GV, GV2GV, etc) has been investigated. Second-order fading statistics of the desired and interference channels have been jointly studied in terms of SIR. Analytical expressions for LCR, AFD, SAC, and CD have been derived for independently and joint characterizing the interference and desired channels. Moreover, mathematical expressions for second-order fading statistics quantifiers for two special cases have been derived, i.e., when the fading rate in the interference channel is much higher and much lower than the desired channel. The proposed framework has been demonstrated as a generalized framework, where a few notable exiting models are its special cases. This generalization of the derived expressions also demonstrates the validity of the conducted study. A comprehensive analysis has been conducted to investigate the impact of various physical parameters. This includes the investigation of the impact of mobility conditions of the communicating and interfering nodes, altitude of the communicating and interfering nodes, elevation of the scattering clusters, fading conditions as defined by the Nakagami shape factor m, and other spatial spread quantifiers on the statistical characteristics of the radio channel. The study emphasises the importance of not excluding the elevation axis while modeling the radio propagation environments and characterizing the fading statistics.

REFERENCES

[1] *System Architecture for the 5G System; Stage 2, Releases 15*, Technical Specification Group Services and Systems Aspects, document 3GPP TS 23.501, V15.2.0, Jun. 2018.

[2] S. J. Nawaz, S. K. Sharma, S. Wyne, M. N. Patwary, and M. Asaduzzaman, "Quantum machine learning for 6G communication networks: State-of-the-art and vision for the future," *IEEE Access*, vol. 7, pp. 46317–46350, Apr. 2019.

[3] M. N. Patwary, S. Junaid Nawaz, M. A. Rahman, S. K. Sharma, M. M. Rashid, and S. J. Barnes, "The potential short- and long-term disruptions and transformative impacts of 5G and beyond wireless networks: Lessons learnt from the development of a 5G testbed environment," *IEEE Access*, vol. 8, pp. 11352–11379, 2020.
[4] M. Shafi, A. F. Molisch, P. J. Smith, T. Haustein, P. Zhu, P. De Silva, F. Tufvesson, A. Benjebbour, and G. Wunder, "5G: A tutorial overview of standards, trials, challenges, deployment, and practice," *IEEE J. Sel. Areas Commun.*, vol. 35, no. 6, pp. 1201–1221, Jun. 2017.
[5] B. Shang, L. Liu, J. Ma, and P. Fan, "Unmanned aerial vehicle meets Vehicle-to-Everything in secure communications," *IEEE Commun. Mag.*, vol. 57, no. 10, pp. 98–103, Oct. 2019.
[6] S. J. Nawaz, A. Ahmed, S. Wyne, K. Cumanan, and Z. Ding, "3-D spatial modeling of network interference in two-tier heterogeneous networks," *IEEE Access*, vol. 5, pp. 24040–24053, Oct. 2017.
[7] S. J. Nawaz, B. H. Qureshi, and N. M. Khan, "A generalized 3-D scattering model for a macrocell environment with a directional antenna at the BS," *IEEE Trans. Veh. Technol.*, vol. 59, no. 7, pp. 3193–3204, Sep. 2010.
[8] C. Ziolkowski and J. M. Kelner, "Angular separation of channels in 5G system multi-beam antennas," in *Proc. Int. Conf. Mil. Commun. Inf. Syst. (ICMCIS)*, May 2019, pp. 1–4.
[9] S. Nawaz, N. Khan, M. Tiwana, N. Hassan, and S. Shah, "Airborne Internet access through submarine optical fiber cables," *IEEE Trans. Aerosp. Electron. Syst.*, vol. 51, no. 1, pp. 167–177, Jan. 2015.
[10] G. D. Durgin and T. S. Rappaport, "Theory of multipath shape factors for small-scale fading wireless channels," *IEEE Trans. Antennas Propag.*, vol. 48, no. 5, pp. 682–693, May 2000.
[11] P. T. Samarasinghe, T. D. Abhayapala, T. A. Lamahewa, and R. A. Kennedy, "Second-order statistics of 2D non isotropic mobile-to-mobile wireless channels," in *Proc. IEEE 22nd Int. Symp. Pers., Indoor Mobile Radio Commun.*, Sep. 2011, pp. 1667–1671.
[12] W. Dahech, N. Hajri, N. Youssef, M. Patzold, and T. Kawabata, "Level-crossing rate and average duration of fades in non-isotropic hoyt fading channels with applications to selection combining diversity," in *Proc. IEEE 82nd Veh. Technol. Conf. (VTC-Fall)*, Sep. 2015, pp. 1–5.
[13] M. I. Akram and A. U. H. Sheikh, "Modeling and simulation of non-isotropic Nakagami Hoyt vehicle to vehicle fading channel," in *Proc. 8th Int. Symp. Commun. Syst., Netw. Digit. Signal Process. (CSNDSP)*, Jul. 2012, pp. 1–6.
[14] M. I. Akram and A. U. H. Sheikh, "On the second order statistics of non-isotropic Nakagami Hoyt mobile to mobile fading channel," *AEU-Int. J. Electron. Commun.*, vol. 67, no. 7, pp. 549–556, Jul. 2013.
[15] M. I. Akram and A. U. H. Sheikh, "On the second order statistical properties of Nakagami Hoyt mobile to mobile fading channel," in *Proc. Australas. Telecommun. Netw. Appl. Conf. (ATNAC)*, Nov. 2011, pp. 1–5.
[16] A. G. Zajic, G. L. Stuber, T. G. Pratt, and S. Nguyen, "Envelope level crossing rate and average fade duration in mobile-to-mobile fading channels," in *Proc. IEEE Int. Conf. Commun.*, 2008, pp. 4446–4450.
[17] E. G. Larsson, O. Edfors, F. Tufvesson, and T. L. Marzetta, "Massive MIMO for next generation wireless systems," *IEEE Commun. Mag.*, vol. 52, no. 2, pp. 186–195, Feb. 2014.
[18] B. Mansoor, S. Nawaz, and S. Gulfam, "Massive-MIMO sparse uplink channel estimation using implicit training and compressed sensing," *Appl. Sci.*, vol. 7, no. 1, p. 63, Jan. 2017.
[19] E. Björnson, L. Sanguinetti, H. Wymeersch, J. Hoydis, and T. L. Marzetta, "Massive MIMO is a reality—What is next?: Five promising research directions for antenna arrays," *Digit. Signal Process.*, vol. 94, pp. 3–20, Nov. 2019.
[20] V. Sharma, M. Bennis, and R. Kumar, "UAV-assisted heterogeneous networks for capacity enhancement," *IEEE Commun. Lett.*, vol. 20, no. 6, pp. 1207–1210, Jun. 2016.
[21] H. Wang, J. Wang, J. Chen, Y. Gong, and G. Ding, "Network-connected UAV communications: Potentials and challenges," *China Commun.*, vol. 15, no. 12, pp. 111–121, Dec. 2018.
[22] H. Q. Ngo, A. Ashikhmin, H. Yang, E. G. Larsson, and T. L. Marzetta, "Cell-free massive MIMO versus small cells," *IEEE Trans. Wireless Commun.*, vol. 16, no. 3, pp. 1834–1850, Mar. 2017.
[23] C. D'Andrea, A. Garcia-Rodriguez, G. Geraci, L. G. Giordano, and S. Buzzi, "Cell-free massive MIMO for UAV communications," in *Proc. IEEE Int. Conf. Commun. Workshops (ICC Workshops)*, May 2019, pp. 1–6.
[24] P. Chandhar and E. G. Larsson, "Massive MIMO for connectivity with drones: Case studies and future directions," *IEEE Access*, vol. 7, pp. 94676–94691, Jul. 2019.
[25] J. Zhang, S. Chen, Y. Lin, J. Zheng, B. Ai, and L. Hanzo, "Cell-free massive MIMO: A new next-generation paradigm," *IEEE Access*, vol. 7, pp. 99878–99888, Jul. 2019.
[26] C. Stefanovic, M. Pratesi, and F. Santucci, "Second order statistics of mixed RF-FSO relay systems and its application to vehicular networks," in *Proc. IEEE Int. Conf. Commun. (ICC)*, May 2019, pp. 1–6.
[27] M. R. Avendi and H. H. Nguyen, "Selection combining for differential amplify-and-forward relaying over Rayleigh-fading channels," *IEEE Signal Process. Lett.*, vol. 20, no. 3, pp. 277–280, Mar. 2013.
[28] H. Ilhan, I. Altunbas, and M. Uysal, "Cooperative diversity for relay-assisted inter-vehicular communication," in *Proc. IEEE Veh. Technol. Conf. VTC Spring*, May 2008, pp. 605–609.
[29] Y. Jin, J. Zhang, S. Jin, and B. Ai, "Channel estimation for cell-free mmWave massive MIMO through deep learning," *IEEE Trans. Veh. Technol.*, vol. 68, no. 10, pp. 10325–10329, Oct. 2019.
[30] E. Chu, J. M. Kim, and B. C. Jung, "Interference analysis of directional UAV networks: A stochastic geometry approach," in *Proc. 11th Int. Conf. Ubiquitous Future Netw. (ICUFN)*, Jul. 2019, pp. 9–12.
[31] J. Zhang, X. Chen, K. P. Peppas, X. Li, and Y. Liu, "On high-order capacity statistics of spectrum aggregation systems over κ–μ and κ–μ shadowed fading channels," *IEEE Trans. Commun.*, vol. 65, no. 2, pp. 935–944, Feb. 2017.
[32] J.-H. Lu and Y. Han, "Application of multipath shape factors in Nakagami-m fading channel," in *Proc. Int. Conf. Wireless Commun. Signal Process.*, Nov. 2009, pp. 1–4.
[33] H.-Y. Shang, Y. Han, and J.-H. Lu, "Statistical analysis of Rician and Nakagami-m fading channel using multipath shape factors," in *Proc. 2nd Int. Conf. Comput. Intell. Natural Comput.*, Sep. 2010, pp. 398–401.
[34] D. Valchev and D. Brady, "Three-dimensional multipath shape factors for spatial modeling of wireless channels," *IEEE Trans. Wireless Commun.*, vol. 8, no. 11, pp. 5542–5551, Nov. 2009.
[35] D. G. Valchev, "Chapter 4: Joint multipath shape factors for modeling mobile-to-mobile channels, thesis title: Spatial modeling of three-dimensional multipath wireless channels," M.S. thesis, Dept. Elect. Comput. Eng., Northeastern Univ., Boston, MA, USA, 2008.
[36] D. Du, X. Jian, X. Wu, Y. Tan, X. Zeng, S. Huang, and Y. Li, "3D spatial characteristics of C-V2X communication interference," *Electronics*, vol. 8, no. 6, p. 718, Jun. 2019.
[37] W. I. Waseer, S. Junaid Nawaz, S. M. Gulfam, and M. J. Mughal, "Second-order fading statistics of massive-MIMO vehicular radio communication channels," *Trans. Emerg. Telecommun. Technol.*, vol. 29, no. 10, p. e3487, Aug. 2018.
[38] Y. Chen, L. Mucchi, R. Wang, and K. Huang, "Modeling network interference in the angular domain: Interference azimuth spectrum," *IEEE Trans. Commun.*, vol. 62, no. 6, pp. 2107–2120, Jun. 2014.
[39] L. Liu, C. Oestges, J. Poutanen, K. Haneda, P. Vainikainen, F. Quitin, F. Tufvesson, and P. Doncker, "The COST 2100 MIMO channel model," *IEEE Wireless Commun.*, vol. 19, no. 6, pp. 92–99, Dec. 2012.
[40] H. C. Nguyen, R. Amorim, J. Wigard, I. Z. Kovacs, T. B. Sorensen, and P. E. Mogensen, "How to ensure reliable connectivity for aerial vehicles over cellular networks," *IEEE Access*, vol. 6, pp. 12304–12317, Feb. 2018.
[41] M. Simunek, P. Pechac, and F. P. Fontan, "Excess loss model for low elevation links in urban areas for UAVs," *Radioengineering*, vol. 20, no. 3, pp. 561–568, Sep. 2011.
[42] J. Karedal, N. Czink, A. Paier, F. Tufvesson, and A. F. Molisch, "Path loss modeling for Vehicle-to-Vehicle communications," *IEEE Trans. Veh. Technol.*, vol. 60, no. 1, pp. 323–328, Jan. 2011.
[43] X. Cai, A. Gonzalez-Plaza, D. Alonso, L. Zhang, C. B. Rodriguez, A. P. Yuste, and X. Yin, "Low altitude UAV propagation channel modelling," in *Proc. 11th Eur. Conf. Antennas Propag. (EUCAP)*, Mar. 2017, pp. 1443–1447.
[44] M. Riaz, N. M. Khan, and S. J. Nawaz, "A generalized 3-D scattering channel model for spatiotemporal statistics in mobile-to-mobile communication environment," *IEEE Trans. Veh. Technol.*, vol. 64, no. 10, pp. 4399–4410, Oct. 2015.
[45] H. Jiang, Z. Zhang, L. Wu, J. Dang, and G. Gui, "A 3-D non-stationary wideband geometry-based channel model for MIMO vehicle-to-vehicle communications in tunnel environments," *IEEE Trans. Veh. Technol.*, vol. 68, no. 7, pp. 6257–6271, Jul. 2019.
[46] S. J. Nawaz, S. Wyne, K. B. Baltzis, S. M. Gulfam, and K. Cumanan, "A tunable 3-D statistical channel model for spatio-temporal characteristics of wireless communication networks," *Trans. Emerg. Telecommun. Technol.*, vol. 28, no. 12, p. e3213, Aug. 2017.

[47] C. Ziolkowski and J. M. Kelner, "Statistical evaluation of the azimuth and elevation angles seen at the output of the receiving antenna," *IEEE Trans. Antennas Propag.*, vol. 66, no. 4, pp. 2165–2169, Apr. 2018.
[48] S. J. Nawaz, N. M. Khan, and R. Ramer, "3-D spatial spread quantifiers for multipath fading wireless channels," *IEEE Wireless Commun. Lett.*, vol. 5, no. 5, pp. 484–487, Oct. 2016.
[49] T. S. Rappaport, *Wireless Communications: Principles and Practice*, vol. 2. Upper Saddle River, NJ, USA: Prentice-Hall, 1996,
[50] L.-F. Huang, "The Nakagami and its related distributions," *WSEAS Trans. Math.*, vol. 15, no. 44, pp. 477–485, 2016.
[51] M. K. Simon and M.-S. Alouini, *Digital Communication Over Fading Channels*, vol. 95. Hoboken, NJ, USA: Wiley, 2005.
[52] M. Nakagami, "The *m*-distribution—A general formula of intensity distribution of rapid fading," in *Statistical Methods in Radio Wave Propagation*. Amsterdam, The Netherlands: Elsevier, 1960, pp. 3–36.
[53] N. Youssef, T. Munakata, and M. Takeda, "Fade statistics in nakagami fading environments," in *Proc. ISSSTA95 Int. Symp. Spread Spectr. Techn. Appl.*, vol. 3, 1996, pp. 1244–1247.
[54] W. C. Lee, *Mobile Communications Engineering*. New York, NY, USA: McGraw-Hill, 1982.
[55] F. Pérez-Fontán and P. M. Espi neira, *Modelling the Wireless Propagation Channel: A Simulation Approach with MATLAB*, vol. 5. Hoboken, NJ, USA: Wiley, 2008.

ALI RAZA received the B.S. degree in electrical engineering from COMSATS University Islamabad, Wah Campus, Pakistan, in September 2018. He is currently pursuing the M.S. degree in electrical engineering with COMSATS University Islamabad, Islamabad Campus, Pakistan.

He has also been working with COMSATS University Islamabad as a Research Assistant, since April 2019. His current research interests include wireless channel modeling, characterizing the interference between mobility nodes, reconfigurable intelligent surfaces, backscatter communication using symbiotic systems, vehicle-to-vehicle communications, massive MIMO systems, and mmWave frequency range and channel estimation using machine learning techniques.

SYED JUNAID NAWAZ (Senior Member, IEEE) received the Ph.D. degree in electronic engineering from Mohammad Ali Jinnah University, Islamabad, Pakistan, in February 2012.

Since September 2005, he has been working on several research and teaching positions with COMSATS University Islamabad (CUI), Islamabad; Staffordshire University, U.K.; Federal Urdu University, Pakistan; the University of York, U.K.; and the Aristotle University of Thessaloniki, Greece. He is currently working as an Assistant Professor with the Department of Electrical and Computer Engineering, COMSATS University Islamabad (CUI). His current research interests include physical channel modeling, channel estimation and characterization, massive MIMO systems, adaptive signal processing, machine learning, compressed sensing, mmWave channels, the airborne Internet, underwater communications, the Internet of Things, and vehicle-to-vehicle communications.

SHURJEEL WYNE (Senior Member, IEEE) received the Ph.D. degree from Lund University, Sweden, in March 2009. Between April 2009 and April 2010, he was a Postdoctoral Research Fellow funded by the High-Speed Wireless Center, Lund University. Since June 2010, he has been with the Department of Electrical and Computer Engineering, COMSATS University Islamabad (CUI), Islamabad, Pakistan, where he serves as an Associate Professor. His research interests include wireless channel characterization, multiantenna systems, cooperative communications, physical layer security, and vehicular communications. He was a co-recipient of the Best Paper Award of the Antennas and Propagation Track at IEEE VTC2013-Spring.

ABRAR AHMED received the B.S. degree in computer engineering from COMSATS University Islamabad, (Formerly, COMSATS Institute of Information Technology) Pakistan, in 2006, the M.S. degree from Lancaster University, U.K., in 2008, and the Ph.D. degree in electrical engineering from COMSATS University Islamabad, in 2017. Since 2006, he has been associated with COMSATS University Islamabad, where he currently holds the position of an Assistant Professor. His research interests include wireless channel modeling and characterizing, smart antenna systems, nonorthogonal multiple access techniques, and adaptive signal processing.

MUHAMMAD AWAIS JAVED (Senior Member, IEEE) received the B.Sc. degree in electrical engineering from the University of Engineering and Technology Lahore, Pakistan, in August 2008, and the Ph.D. degree in electrical engineering from The University of Newcastle, Australia, in February 2015. From July 2015 to June 2016, he worked as a Postdoctoral Research Scientist with the Qatar Mobility Innovations Center (QMIC) on the SafeITS Project. He is currently working as an Assistant Professor with COMSATS University Islamabad, Pakistan. His research interests include intelligent transport systems, vehicular networks, protocol design for emerging wireless technologies, and the Internet of Things.

MOHAMMAD N. PATWARY (Senior Member, IEEE) received the B.Eng. degree (Hons.) in electrical and electronic engineering from the Chittagong University of Engineering and Technology, Bangladesh, in 1998, and the Ph.D. degree in telecommunication engineering from The University of New South Wales at Sydney, Sydney, NSW, Australia, in 2005. He was with General Electric Company, Bangladesh, from 1998 to 2000, and Southern Poro Communications, Sydney, from 2001 to 2002, as a Research and Development Engineer. He was a Lecturer with The University of New South Wales at Sydney, from 2005 to 2006, and then a Senior Lecturer with Staffordshire University, U.K., from 2006 to 2010. He was then a Full Professor of wireless systems and digital productivity and the Chair of the Centre of Excellence on Digital Productivity With Connected Services, Staffordshire University, until 2016. He is currently a Full Professor of telecommunication networks and digital productivity and the Head of the Intelligent Systems and Networks (ISN) Research Group, School of Computing and Digital Technology, Birmingham City University, U.K. He is also a Principal Data Architect for a large scale 5G testbed in the U.K. to accelerate digital productivity and to develop urban connected community. His current research interests include sensing and processing for intelligent systems, wireless communication systems design and optimization, signal processing and energy-efficient systems, future generation of cellular network architecture, and business modelling for data-economy.